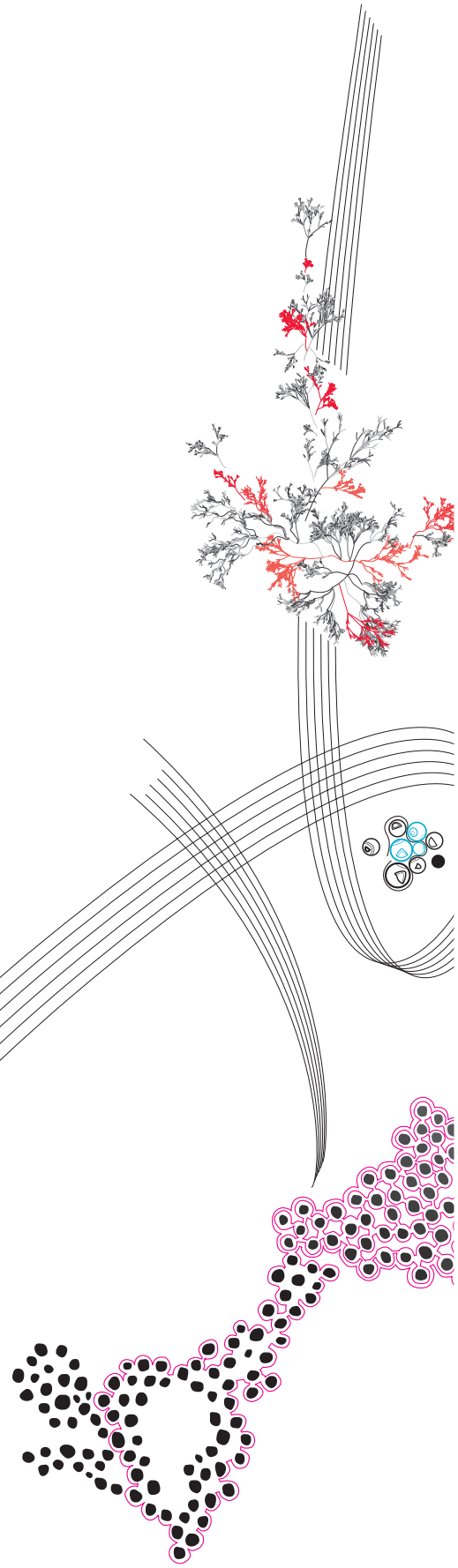

MSc Thesis Biomedical Engineering

Physical Activity Energy Expenditure Estimation in Activities of Daily Living using a Simplified Physiological Computing Model

R.J. Poelarends

Supervisors:
Peter Veltink
Ying Wang
Ramon Que
Gjerrit Meinsma

June, 2024

Department of Biomedical Signals and Systems
Faculty of Electrical Engineering,
Mathematics and Computer Science

UNIVERSITY OF TWENTE.

Physical Activity Energy Expenditure Estimation in Activities of Daily Living using a Simplified Physiological Computing Model

R. J. Poelarends*

June, 2024

*Email: r.j.poelarends@student.utwente.nl

Abstract

Introduction:

With over one billion people suffering from obesity, addressing energy imbalance between calories consumed and expended is critical. A tailored and dynamic model is essential for providing personalized insights into energy expenditure patterns, especially for development of personalized obesity interventions. In this study, we aimed to develop a simplified physiological computing model to accurately estimate physical activity energy expenditure (PAEE).

Methods:

An observational study was conducted at the eHealth House, University of Twente, involving 10 participants aged 23 - 49. Participants performed various activities of daily living monitored by multiple wearable sensors. A simplified three-compartment model was utilized, incorporating the lungs, circulation system, and muscle tissue. The model estimated PAEE using heart rate and inertial measurement unit (IMU) data as inputs. Two model variations were tested: model 1 utilized pelvis IMU data, and model 2 integrated IMU data from both the pelvis and thighs. Performance metrics were coefficient of determination (R^2) and root mean square error (RMSE).

Results:

Model 1 exhibited a significantly lower mean R^2 compared to model 2 (0.256 ± 0.302 vs. 0.375 ± 0.312, p=0.05). No significant difference was found between model 1 and model 2 in terms of RMSE (0.112 ± 0.035 kJ/min/kg vs. 0.100 ± 0.037 kJ/min/kg, p = 0.08). In terms of RMSE, both models performed significantly worse on the cycling activity for each participant, compared to the other activities.

Discussion/Conclusion:

In this study, we presented a promising approach for PAEE estimation using a simplified physiological computing model, accounting for individual physiological differences and the dynamics of energy expenditure. By integrating wearable sensor data with physiological principles, our method might offer a significant advancement in personalized health monitoring and obesity research, paving the way for more effective interventions and lifestyle improvements.

Keywords: Physical Activity Energy Expenditure; Energy Expenditure; Physical Activity; Wearable Sensors; Personalized Health; Activities of Daily Living.

Contents

1 Introduction

In 2020, over 38% of the world population aged over 5 years was classified as overweight and 14% were diagnosed with obesity. According to the World Obesity Atlas, these numbers are expected to increase to 51% and 24% in 2035, respectively [1]. The fundamental cause of obesity and overweight lies in the energy imbalance between calories consumed and expended. The imbalance is fuelled by the widespread consumption of energy-dense, ultra-processed foods along with rising physical inactivity [2]. Insight into energy expenditure (EE) could help people increase physical activity (PA) and improve their lifestyle.

Total daily EE (TEE) encompasses the sum of energy expended by the body during a 24-hour period, reflecting the energy expenditure of several components. Basal metabolic rate (BMR) is responsible for 60-70% of TEE and refers to the energy required to maintain essential bodily functions. Physical activity energy expenditure (PAEE) is the energy expended during PA, representing 15-30% of TEE. Diet-induced thermogenesis (DIT) represents 10% of TEE and reflects the energy required to digest, absorb, and metabolise eaten food [3]. TEE can be measured using the doubly-labeled water (DLW) method or calorimetry (direct or indirect) [4], while the BMR can be estimated by calorimetry (direct or indirect) under fasting and resting conditions [5]. It is important to gain information about an individual's PAEE, as it is the most variable component of TEE. Using estimations of these components, PAEE can be calculated as TEE minus BMR and DIT. However, these methods are expensive and unusable in daily life [6].

As a result, there is an increased focus on the development of sensor-based monitoring tools for PAEE. Such tools offer a tailored approach for PAEE estimation by using one or multiple accelerometers, sometimes in combination with anthropometric characteristics, gyroscopes or a heart rate sensor [7, 8]. The spectrum of existing approaches spans from simple linear models to complex non-linear models [7, 9]. The systematic review by Jeran *et al.* revealed a variance in activity-related EE explained by accelerometer-assessed physical activity ranging from 12.5-86% under free-living conditions [8]. Furthermore, it highlighted that 22 out of 28 selected papers employed a linear prediction model, with a majority of the models using counts/interval as the input. The variance in TEE during activities of daily living (ADL) explained by IMU and HR data ranged from 38-85%, according to Hedegaard *et al.* [7]. Linear models performed worse compared to non-linear models, such as a cubic model or an artificial neural network. Notably, studies have shown that combining accelerometer, gyroscope, and heart rate data increases EE estimation accuracy [10, 11, 12]. To further enhance the performance of these models, a common strategy involves combining an estimator with an activity recognition algorithm, due to the inability of single estimators to generalize on different activity types [11, 13].

However, the above-mentioned studies utilized PAEE estimation models that often lack explainability and personalization capabilities. These models, while effective in predicting PAEE to a certain level, fail to provide insights into the underlying physiological mechanisms governing PAEE variability among individuals. These limitations hinder the interpretability and trustworthiness of the models, which is a critical requirement for their practical application in real-world healthcare settings. Without explainability, healthcare professionals may find it challenging to fully trust the predictions made by these models, potentially limiting their adoption. Furthermore, the lack of personalization capabilities in currently published models limits the capacity to reflect the unique physiological char-

acteristics of each user, leading to less accurate PAEE estimations. This is especially the case during ADL, where variability in PAEE can be large and context-specific.

To address these limitations of existing PAEE estimation models, we propose a novel approach that integrates a physiological model of energy expenditure, laws of physics, and sensor data through a simplified physiological computing model. This approach accounts for individual differences in physiology, activity levels, and body composition, leading to more accurate and interpretable PAEE estimates for individuals. In addition, the integration of sensor data, such as accelerometers and heart rate, enables real-time and accurate monitoring of PAEE during ADL [7]. We aim to develop a personalized PAEE estimation tool that can be used during ADL, providing users with accurate insights into their energy expenditure patterns. The main focus of my master's project was the exploration of PAEE modelling during ADL and developing a model that is both transparent and understandable.

2 Methods

2.1 Study design

We conducted an experiment to collect a realistic and diverse dataset with multiple sensors and high sampling frequency, providing an accurate and realistic representation of energy expenditure during ADL. This observational study was conducted at the eHealth House, University of Twente. Participants were observed performing various activities of daily living for 50 minutes.

2.1.1 Study population

We recruited 10 participants (30% female) for this study. Inclusion criteria were: (1) aged between 18 and 60 [14]; (2) have a Body Mass Index (BMI) lower than 40 kg/m^2 [15]; (3) free of cardiovascular diseases, respiratory diseases, metabolic disorders; (4) not being pregnant; (5) free of physical disabilities that impact daily living. Participants agreed to the use of their anonymized recorded data for scientific research.

2.1.2 Data collection

The experiment was ethically approved by the Ethics Committee Computer & Information Science of the University of Twente (reference number 230728). Informed consent was obtained from all individual participants included in the study. The eHealth House was equipped with cameras and microphones to monitor and record participants' activities [16]. A map of the facility is provided in Figure 1.

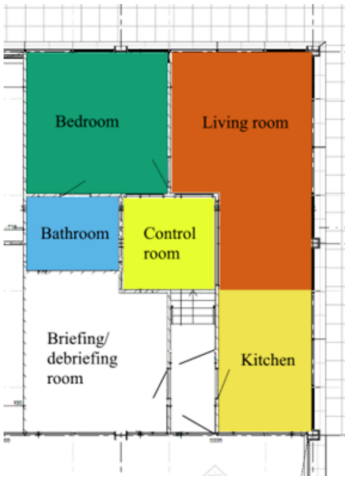

Figure 1: Floor map of eHealth House [16]

Participants performed a series of activities of daily living, categorized into sedentary (low whole-body motion (LWBM)) and non-sedentary (walking, biking, and high whole-body motion (HWBM)) activities for approximately 50 minutes [17]. Static data such as age, sex, height, and weight, were collected. Body composition was estimated using a Bioelectrical Impedance Analysis (BIA) scale (Omron BF511). Quality of Life (QoL) information was collected using the 36-Item Short Form Survey (SF-36) and information about recent physical activity levels was collected using the International Physical Activity Questionnaire (IPAQ) [18, 19]. Emotional states and mood over the past week were measured using the Positive and Negative Affect Schedule (PANAS) questionnaire.

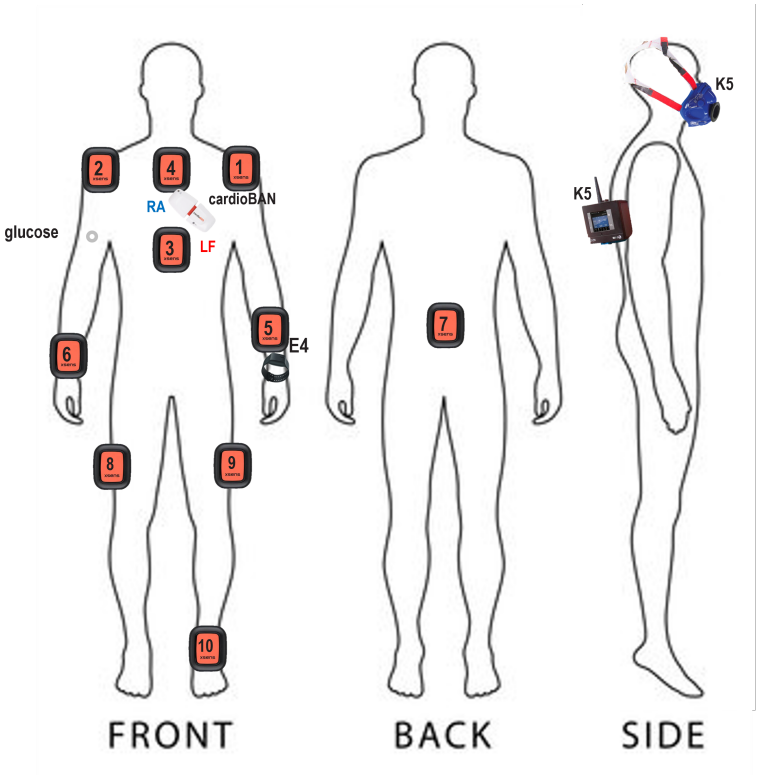

Figure 2: Distribution of the used sensors.

Objective data was captured using different wearable sensors. IMU data was collected at 30 Hz at ten body locations, e.g. left shoulder, right shoulder, chest, sternum, pelvis, left thigh, right thigh, left wrist, right wrist, and on the shoe at the dominant leg [11] (Movella Xsens DOT [20]). Single-lead ECG data was collected (CardioBan Kit [16]) at 80 Hz, and additional physiological data, including photoplethysmogram (PPG), electrodermal activity (EDA), 3-axis accelerometer and skin temperature, were measured using a smartwatch (Empatica E4 [21]). Also, glucose levels were continuously recorded (Freestyle Libre 3 [22]) Breath-by-breath respiratory data, serving as ground truth, was collected (COSMED K5 [23]) and activity labels were added using the OMNIA COSMED software. The sensor distribution is shown in Figure 2.

2.1.3 Pre-experimental conditions

To estimate the Rest Metabolic Rate (RMR) as accurately as possible, it was necessary to get as many body systems as possible at rest, such as systems for digestion and muscle recovery. Due to this, participants were asked to refrain from eating 7 hours before the experiment. They were allowed to eat a small meal (<300 kcal) at most 2 hours before the experiment, so the participants received a couple of example recipes of meals containing less than 300 kcal. To make the Diet-Induced Thermogenesis (DIT) component approach zero, participants were asked to avoid caffeine and other stimulants for at least 4 hours before the experiment and avoid nicotine for at least 2.5 hours before the experiment. Finally, the participants were asked to refrain from vigorous physical activities for at least 24 hours before the experiment. This was done to make sure that the PAEE component approached zero in absolute rest [24]. These instructions are the minimal requirements for reliable RMR estimation. During the entire session, the thermostat was set to 22° Celsius

Table 1: List of activities with corresponding duration. x represents variable activity duration.

Cluster	Activity	Duration in seconds
LWBM	Sitting resting	300
	Sitting reading	300
	Standing still	180
	Working on a laptop	x
HWBM	Emptying dishwasher	x
	Mopping	x
	Stacking shelves with books	x
Walking	Climbing stairs (5 times)	x
	Treadmill (3 km/h)	300
	Treadmill (5 km/h)	300
Cycling	Cycle at 125 Watt	300

to reduce the energy expenditure of cold-induced thermogenesis [24].

2.1.4 Experimental procedure

The session commenced with a 30-minute quiet rest in supine position to estimate rest metabolic rate (RMR) [25]. This was followed by a series of daily living activities. Most activities were performed for at least 5 minutes to reach steady-state EE, as recommended by [26]. For HWBM activities, climbing stairs, and working on a laptop, the participants were instructed to execute the activities at their own speed, which made the duration of these activities variable. The surveys were filled in on the laptop during the 'working on a laptop' activity. Breaks between activities were not predetermined and were up to the participant. Each participant performed the activities in randomised order to prevent the introduction of bias in the dataset [9]. The randomization and the variable duration of the HWBM activities help to simulate real situations of daily living. The activities and their duration are presented in Table 1. The order of activities for each participant is presented in the appendix in Section A.4.

2.2 Data preprocessing

To estimate the RMR in terms of VO_2 and VCO_2, the initial 5 minutes of the RMR measurement were excluded to eliminate any transient effects from the onset of the resting period. The average VO_2 and VCO_2 were calculated from the remaining data, as instructed by Compher *et al.* [27]. These averages were considered representative of the participant's RMR. The measured TEE during the ADL consists of the components PAEE and RMR. The average RMR VO_2 and VCO_2 were subtracted from the TEE, which is the preprocessed VO_2 and VCO_2 measurements during the ADL. PAEE was then derived using the following equation:

$$\text{PAEE} = \text{TEE} - \text{RMR} \tag{1}$$

Where PAEE denotes physical activity energy expenditure, TEE denotes total energy expenditure, and RMR denotes rest metabolic rate energy expenditure. All components have the unit kJ.

For heart rate detection, a modified Pan & Tompkins detection algorithm by Thoonen *et al.* was used [28]. The heart rate signal was smoothed using a first order Savitzky-Golayfilter with a 20-second window length. This window length was chosen empirically, as it provided the best balance between noise reduction and preservation of signal details. Then, the heart rate signal was resampled to 1 Hz. The breath-by-breath VO_2 and VCO_2 data was first resampled to 1 Hz, as the sampling rate was equal to the breathing rate and thus variable. To remove noise and correct for artefacts caused by talking, the breath-by-breath signals were smoothed using a first order Savitzky-Golayfilter with a 20-second window length. The raw acceleration data collected from the IMU sensor includes the influence of gravity. To isolate the participant-generated acceleration, we first defined a standard gravity vector $[0, 0, 9.81]$ m/s^2 representing the gravitational acceleration. The vector was inversely rotated using the quaternion representation of the sensor's orientation to align it with the IMU coordinate system. The resulting vector was subtracted from the raw acceleration data to correct for the gravitational acceleration. Subsequently, a Butterworth 8th-order bandpass filter with cut-off frequencies between 0.5 and 5 Hz was utilized to filter the acceleration data, as the performed ADL are expected to have acceleration within the range of 0.5 and 5 Hz. The velocity was estimated for each direction by cumulatively integrating the signal using the composite trapezoidal rule. As velocity might not get to zero at rest after integration due to remaining noise in the filtered linear acceleration, the velocity is set to zero whenever the filtered linear acceleration is zero for a period of 5 consecutive samples [29]. The magnitude of the velocity vector was calculated to represent the velocity of the IMU sensor. Finally, all signals were synchronized and resampled to 1 Hz. The preprocessing workflow of all signals is shown in Figure 3.

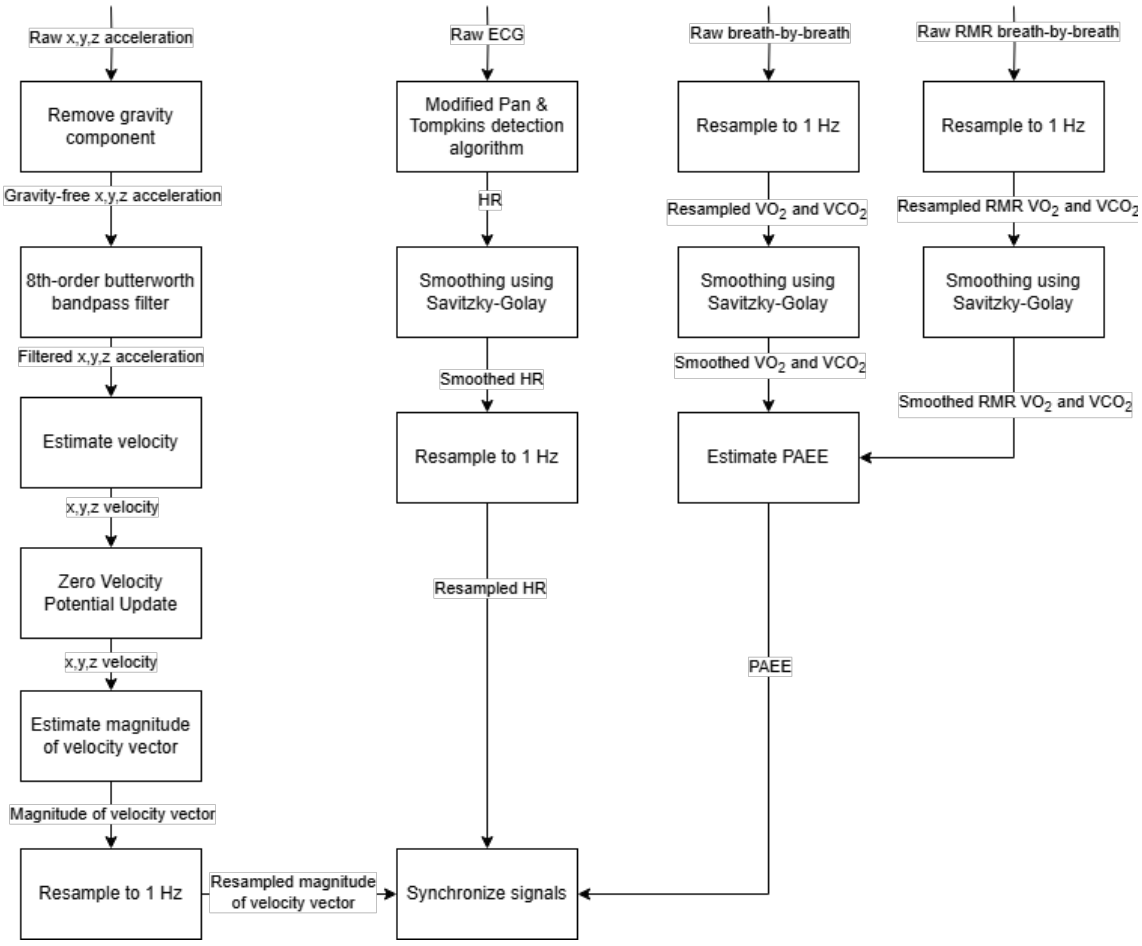

Figure 3: Preprocessing workflow of acceleration, ECG, and breath-by-breath data. The breath-by-breath data for the RMR measurement follows the same processing pipeline as the breath-by-breath data during the ADL. The 'Estimate PAEE' block represents Equation 1. HR denotes heart rate, RMR denotes rest metabolic rate, and PAEE denotes physical activity energy expenditure.

2.3 Model formulation

Energy expenditure can be estimated through indirect calorimetry, which estimates the amount of energy using the volume of inhaled and exhaled oxygen (O_2) and carbon dioxide (CO_2). O_2 and CO_2 are moved via the blood circulation system to the muscles, which determine the demand of O_2 and the production of CO_2. Therefore, the model to estimate physical activity energy expenditure from movement data is composed of three compartments, representing the lungs, the circulation system and muscle tissue.

2.3.1 Qualitative model description

This three-compartment control system was built upon a simplification of the model introduced in [30]. A schematic diagram of the controlled three-compartment system is demonstrated in Figure 4.

The lung compartment represents the exchange of $O2$ and $CO2$ between the air in the lungs and the bloodstream, facilitated by the pulmonary alveoli. The lung was modelled as a collection of alveoli in which the alveolar gas volume (V_A) represents the available space in the alveoli for gas exchange. The total ventilation ($\dot{V}_A$) dictates the air volume flowing in and out of the lungs in liters per second. The total ventilation was adjusted using a respiratory controller when levels of O_2 and CO_2 deviated from basal values. The differences between partial pressures of O_2 (P_{I,O_2}) and CO_2 (P_{I,CO_2}) of the inhaled air and the partial pressures of O_2 (P_{A,O_2}) and CO_2 (P_{A,CO_2}) in the alveoli results in changes of the partial pressures in the alveoli.

The circulation system represents the transport of O_2 and CO_2 from the arteries in the lungs to the tissue and back. The cardiac output (Q) determines the diffusion rate of O_2 and CO_2 between the blood and the alveoli or tissue by regulating the volume of blood flowing through the pulmonary and systemic circulations, where gas exchange occurs. A small fraction of the venous blood does not reach the lungs but passes through the pulmonary shunt. This fraction of blood is described as the pulmonary shunt fraction p_s. The blood going through the pulmonary shunt with venous concentration (C_v) and through the lungs with end-capillary concentration (C_e) comes together at the arteries. The arterial concentration (C_a) was described as the weighted sum of C_v and C_e.

The tissue compartment represents the skeletal muscle tissue that generates force for movement during physical activities. The skeletal muscle tissue has a volume (V_T) and a concentration of O_2 and CO_2. The concentration in the tissue was altered by the metabolic production rate (R_M) of O_2 and CO_2, which represents the required energy for the generated force in terms of O_2 demand and CO_2 production. R_M was estimated using inertial measurement unit (IMU) data and converted using laws of physics to physiological interpretable values.

2.3.2 Assumptions and symbols

The model was built upon several key assumptions:

1. The system consists of three compartments: the lungs, the circulation system, and the tissue.

2. The system consists of two reservoirs: the lungs, and the tissue.

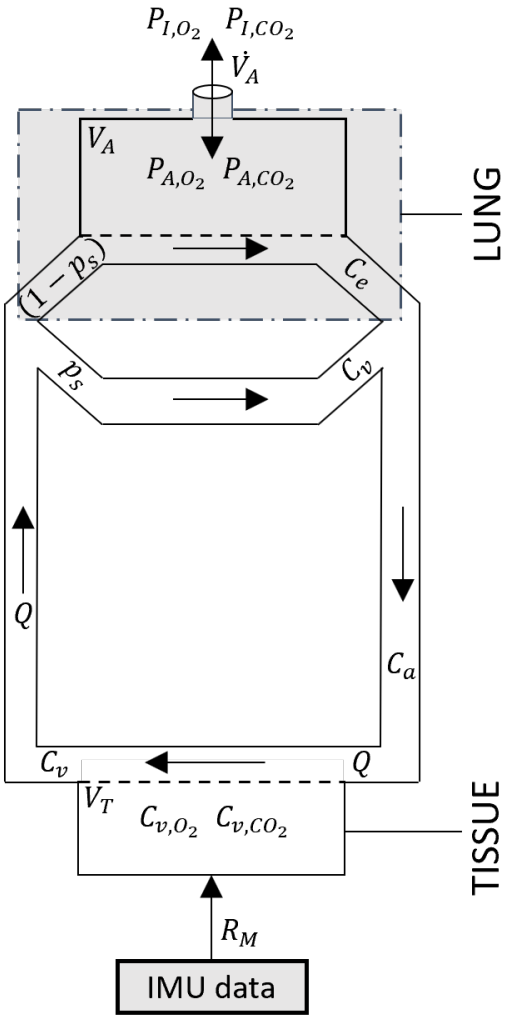

Figure 4: Functional block diagram of the three-compartment respiratory system. P_{I,O_2} denotes partial O_2 pressure of inspired gas in $mmHg$; P_{I,CO_2} denotes partial CO_2 pressure of inspired gas in $mmHg$; $\dot{V}_A$ denotes total ventilation in L/s; V_A denotes alveolar gas volume in liter; P_{A,O_2} denotes alveolar partial O_2 pressure in $mmHg$; P_{A,CO_2} denotes alveolar partial CO_2 pressure in $mmHg$; p_s denotes the dimensionless pulmonary shunt fraction; C_e denotes end-capillary concentration in liter O_2 or CO_2 per liter blood; C_v denotes venous concentration in liter O_2 or CO_2 per liter blood; C_a denotes arterial concentration in liters O_2 or CO_2 per liter blood; Q denotes cardiac output in L/s; V_T denotes tissue volume in liters; C_{v,O_2} denotes venous O_2 concentration in liter O_2 per liter blood; C_{v,CO_2} denotes venous CO_2 concentration in liter CO_2 per liter blood; R_M denotes metabolic production rate in L/s.

3. Lung and tissue volumes remain constant.

4. The reservoirs have uniform tissue composition with a homogeneous concentration and partial pressure distribution.

5. Pressure and concentration changes within the reservoirs occur uniformly and instantaneously.

6. Blood flow within the circulation system is steady and continuous with uniform concentration distribution.
7. Gas behaviour within the lungs adheres to the principles of the ideal gas law.
8. Gas exchange at the alveoli occurs without limitation.
9. Alveolar ventilation is controlled by peripheral chemoreceptors using C_{a,O_2} and P_{A,CO_2}.
10. Blood pH is maintained within the physiological range, allowing for normal gas exchange.
11. Dissociation curves are equal for arterial and venous blood.
12. The respiratory quotient is constant.

It is neither practical nor necessary to include specific details about the process of energy expenditure as the complexities of physiological responses and biochemical pathways are beyond the scope of the measured data. Instead, the model focuses on the macroscopic view of energy dynamics, relying on measurements that reflect overall system behaviour. Assumptions 1 to 3 ensure that the model does not need to account for variable changes in size or heterogeneous distributions, which would significantly complicate the mathematical representation and computational requirements. Assumptions 4 and 5 help to avoid the need for differential equations that would otherwise be required to describe gradients or time delays in gas exchange. Assumption 6 is necessary to avoid the complexities of pulsatile flow and the resulting gas variations in gas transport rates. This allows for O_2 and CO_2 transport. Assumption 7 is a well-established principle in physics which allows us to simplify the equations that describe gas behaviour. In reality, gas exchange can be influenced by many factors, which would add very complex details. Using assumption 8, the model can focus on the primary factors that drive gas transport. Assumption 9 simplifies the complex regulatory mechanisms of the respiratory systems. The peripheral chemoreceptors are sensitive to changes in C_{a,O_2} and P_{A,CO_2}, which are the primary stimuli that affect breathing. Assumption 10 allows the model to avoid the need to account for the effects of acid-base balance on gas transport and metabolism, which simplifies the model. Assumption 11 simplifies the model by not differentiating between the O_2 and CO_2 carrying capacities of blood. In reality, these curves differ due to various physiological factors, but treating them as equal allows for a more straightforward calculation of gas exchange without the need for additional data. Finally, assumption 12 is a standard simplification in metabolic studies, as the respiratory quotient can vary with diet, type of cellular respiration, and other factors. With our current measurements, it is not possible to estimate this value for each individual, as it requires more complex data.

2.4 Mathematical model

This section describes the equations governing each subsystem of the model, starting with the introduction of the balance equations for the lung and tissue compartment, which describe how gases are transported and utilized within the body. Following this, the respiratory controller is described. Subsequently, the used methods for estimating output ventilation values and calculating energy expenditure are discussed. Next, the utilization of IMU data to compute the metabolic production rate of O_2 and CO_2, serving as model input, is explained. The final subsection describes adjustments to tailor the model for performance enhancement.

A full list of the used symbols and associated units are given in the appendix in Table 8. All empirical constants are defined in the text.

2.4.1 Balance Equations for Lung and Tissue Compartment

Balance equations describe the conservation of mass for O_2 and CO_2 in a compartment. The equations serve as a mathematical representation of how gases are transported and utilized within the body. The balance equations are identical for O_2 and CO_2. For clarity, a subscript indicating the chemical species (either O_2 or CO_2) is omitted in Equations 2 to 4. In developing equations 2 to 4, we have utilized the equations presented by Chiari *et al.* in [30], with modification to the notation for consistency with the framework used in this report.

The bloodstream in the pulmonary capillaries and gas flow in the lungs are assumed to be continuous and unidirectional in the lung compartment. Changes in P_A can result from differences between partial pressures in the inhaled air and alveolar partial pressures, scaled by alveolar ventilation, and from differences between venous and end-capillary concentrations, scaled by the blood flow. Alveolar ventilation determines the exchange of gases in the lungs, influencing the pressure gradient across the alveolar membrane. Meanwhile, blood flow regulates the transport of substances in the bloodstream, affecting the concentration gradient between venous and end-capillary blood. The magnitude of the change in P_A is dependent on the volume of the compartment and therefore proportionally scaled by the alveolar volume. The following equation describes the alveolar partial pressure P_A:

$$V_A \cdot \frac{dP_A}{dt} = \dot{V}_A \cdot (P_I - P_A) + \lambda \cdot Q \cdot (1 - p_s) \cdot (C_v - C_e) \tag{2}$$

Where V_A is the alveolar gas volume and P_I is the partial pressure of O_2 or CO_2 in the inspired gas. C_v and C_e are venous and end-capillary concentrations of O_2 and CO_2. λ is a coefficient that converts blood concentrations into alveolar partial pressure, Q is the cardiac output, and p_s represents the pulmonary shunt, giving a constant fraction of venous blood that does not reach the alveoli.

The concentration in the tissue compartment is assumed to be equal to the concentration in venous blood. The concentration in tissue changes when there is a difference in concentrations in venous and arterial blood, or when R_M is not zero. Non-zero R_M represents elimination of O_2 or production of CO_2 in the tissue compartment, resulting in a change of concentration in tissue. The blood flow affects the concentration gradient between venous and end-capillary blood, similar to the relationship observed in the lung compartment. The magnitude of the change in C_v is dependent on the volume of the compartment and therefore proportionally scaled by the tissue volume. The equation below governs the mass balance in the tissue compartment:

$$V_T \cdot \frac{dC_v}{dt} = Q \cdot (C_a - C_v) + R_M \tag{3}$$

Where V_T and C_v are the volume and gas concentrations in the tissue, respectively. C_a represents the arterial concentration. R_M is the metabolic production/elimination rate of gas, which is positive for CO_2 and negative for O_2.

The venous blood flowing through the pulmonary shunt and blood flowing through the lungs come together, resulting in arterial blood. It is assumed that venous blood concentrations are constant when flowing to the lungs. Arterial gas concentration is calculated

by the shunt equation:

$$C_a = (1 - p_s) \cdot C_e + p_s \cdot C_v \tag{4}$$

Where C_a, C_e and C_v denote the arterial blood concentration, end-capillary concentration and venous blood concentration, respectively. p_s represents the fraction of blood flowing through the pulmonary shunt and $(1 - p_s)$ represents the fraction of blood flowing through the lungs.

2.4.2 O_2 and CO_2 Dissociation Curves

To solve equations 2 to 4, the concentrations O_2 and CO_2 in blood were deduced from the partial pressures. It is assumed that alveolar pressure is equal to end-capillary pressure ($P_A = P_e$). Dissociation curves from Fincham *et al.* [31] were used to convert partial pressures to concentrations:

$$C_{O_2} = K_2(1 - e^{-K_3 \cdot P_{O_2}})^2 \tag{5}$$

$$C_{CO_2} = K_4 \cdot P_{CO_2} \tag{6}$$

Where C_{O_2} and C_{CO_2} represent a concentration of O_2 and CO_2, respectively. P_{O_2} and P_{CO_2} represent corresponding partial pressure of O_2 and CO_2. K_2, K_3 and K_4 represent constants determined through a linear best fit.

2.4.3 The Respiratory Controller

The respiratory control system adjusts alveolar ventilation based on deviations from basal levels of O_2 and CO_2. The physiological respiratory control centre consists of several linked controllers, processing many different inputs. The actions of the controller mainly depend on the contribution of the peripheral chemoreceptors, which respond rapidly to changes in P_{A,CO_2} and C_{a,O_2}, and the central chemoreceptors, which are sensitive the medullary CO_2 tension. For simplification, we accounted only for the influence of peripheral chemoreceptors, given that they respond faster than the central chemoreceptors and are sensitive to changes in both O_2 and CO_2.

The contribution of peripheral chemoreceptors to $\dot{V}_A$ depends on both C_{a,O_2} and P_{A,CO_2}. Based on experimental observations, it has been found that ventilation is a linear function of P_{A,CO_2} at a constant level of C_{a,O_2}, and that ventilation is a linear function of C_{a,O_2} at a constant level of P_{A,CO_2} [32].

The contribution of peripheral chemoreceptors to $\dot{V}_A$ is described using the following equation, which is a simplified version of the controller presented by Chiari *et al.* in [30]:

$$\frac{d\dot{V}_A}{dt} = -G_{p,O_2} \cdot C_{a,O_2} + G_{p,CO_2} \cdot P_{A,CO_2} + K_1 \tag{7}$$

Where $\dot{V}_A$ represents the alveolar ventilation, and G_{p,O_2} and G_{p,CO_2} represent the proportional gains in the controller. Parameter K_1 was assigned to have $\dot{V}_A = \dot{V}_0$ in basal conditions, where $\dot{V}_0$ denotes the basal alveolar ventilation value.

To prevent ventilation from reaching negative values, as this is physiologically unattainable, ventilation is automatically set to zero whenever its value falls below zero.

$$\dot{V}_A = \begin{cases} \dot{V}_A, & \dot{V}_A \geq 0 \\ 0, & \dot{V}_A < 0 \end{cases} \tag{8}$$

2.4.4 Ventilation

For energy expenditure estimation, the exhaled VO_2 and VCO_2 per second, $\dot{V}_{O_2}$ and $\dot{V}_{CO_2}$, needs to be estimated. The exhaled gas volumes can be estimated using gas volumes of alveolar ventilation. The exhaled gas volumes by alveolar ventilation can be estimated as the product exhaled volume and the difference in gas fraction of inhaled and exhaled air, for O_2 and CO_2. The gas fraction of exhaled air was estimated using the alveolar gas equation [33], which is substituted in Equations 9 and 10. To estimate the exhaled $\dot{V}_{O_2}$ and $\dot{V}_{CO_2}$ per second, we utilized the following equations:

$$\dot{V}_{O_2} = \dot{V}_A \cdot (F_{I,O_2} - \frac{P_{A,O_2}}{P_{atm} - P_{H_2O}}) \tag{9}$$

$$\dot{V}_{CO_2} = \dot{V}_A \cdot (F_{I,CO_2} - \frac{P_{A,CO_2}}{P_{atm} - P_{H_2O}}) \tag{10}$$

Where F_IO_2 and F_ICO_2 are the partial gas fractions of inhaled air, P_{A,O_2} and P_{A,CO_2} are the alveolar pressures of O_2 and CO_2. P_{atm} denotes the atmospheric pressure at sea level and P_{H_2O} denotes the partial pressure of water in the alveoli, which is used to correct for the humidity levels in the alveoli.

Weir's formula [34], considered the gold standard for energy expenditure estimation using indirect calorimetry, estimates TEE and RMR using measurements of $\dot{V}_{O_2}$ and $\dot{V}_{CO_2}$. It utilizes fundamental principles of metabolism and a regression model to estimate energy expenditure. The equation has served as a reference method to assess the accuracy of other methods for energy expenditure estimation, such as accelerometers or predictive equations for resting energy expenditure [35].
The measured TEE consists of the components PAEE and RMR. PAEE was derived using the following equation:

$$\text{PAEE} = \text{TEE} - \text{RMR} \tag{11}$$

Where PAEE denotes physical activity energy expenditure, TEE denotes total energy expenditure, and RMR denotes rest metabolic rate energy expenditure. All components have the unit kJ.
A critical assumption for Weir's formula is the negligible contribution of anaerobic metabolism for the duration of the measurement, an assumption that holds for low- and moderate-intensity activities but may not be accurate for high-intensity exercises. Given this limitation, Weir's formula was used to estimate TEE and BMR:

$$EE = 3.9 \cdot V_{O_2} + 1.1 \cdot V_{CO_2} \tag{12}$$

Where V_{O_2} denotes the net volume of O_2 per second, and V_{CO_2} denotes the net volume of CO_2 per second.

2.4.5 Metabolism

For the estimation of R_M, we estimated the amount of energy that it takes to move the body with a certain velocity. The estimated energy is converted to metabolic demand/production of O_2 and CO_2 using the respiratory quotient (RQ). This approach holds under the assumption that metabolic demand and production approach zero after a period in which none of the body components was moved. This can be assumed because PAEE is estimated, which does not include the maintenance energy cost of tissue.
Several IMUs were connected to different segments of the subject's body. Using this approach, the required energy to move a body segment was estimated. The velocity v of the centre of mass (CoM) of a segment was estimated by integrating the IMU data, under the assumption that the IMU is attached to the CoM. The required energy to move the body within a timestep was calculated using the equation for kinetic energy. As the muscles are not 100% efficient, the kinetic energy will be an underestimation of the actual energy used. To correct the kinetic energy for human muscle efficiency, the energy is scaled by the human muscle efficiency factor.

$$E(t) = \frac{\frac{1}{2} \cdot M_B \cdot v^2(t)}{\mu} \tag{13}$$

Where M_B is the total mass of the body, v is the total velocity of the CoM of the segment, and μ denotes the human muscle efficiency percentage.

The energy was then converted to the metabolic demand of O_2 using the conversion factor of 19.6 kJ, given that one litre O_2 produces 19.6 kJ of heat [36]. For this, it was assumed that activities of daily living fall within aerobic energy expenditure levels. The metabolic production rate of CO_2 was calculated using the RQ, which is the ratio of carbon dioxide (VCO_2) production to oxygen (VO_2) consumption. RQ is an indicator of metabolic fuel use in tissues and typically ranges between 0.7 and 1.0. We assumed an RQ of 0.8, which summarizes a mixture of consumed substrates (carbohydrates, fat, and protein). The metabolic production rate of oxygen (R_{M,O_2}) and carbon dioxide (R_{M,CO_2}) were estimated as follows:

$$R_{M,O_2}(t) = \frac{E(t)}{19.6} \tag{14}$$

$$R_{M,CO_2}(t) = 0.8 \cdot R_{M,O_2}(t) \tag{15}$$

Where R_{M,O_2} and R_{M,CO_2} represent the metabolic demand of O_2 and the metabolic production of CO_2, respectively.

2.4.6 Model tailoring approach

As energy expenditure has a high variability between humans, tailoring the model was expected to improve the performance. Certain constants in the model were assigned values obtained from individual-specific measurements. In addition, one variable was estimated using machine learning to optimize model performance.

Subject-dependent constants The body mass (M_B), the muscle volume (V_T), and the cardiac output (Q) were made subject-dependent and based on collected data. The mass M_B used to calculate the kinetic energy equalled the mass of the subject.

The muscle volume V_T was calculated using the density of skeletal muscle as follows:

$$V_T = M_{SM} \cdot \rho \tag{16}$$

Where M_{SM} dentes the measured skeletal muscle mass, and ρ denotes the density of skeletal muscle mass.

The cardiovascular compartment was included in the circulation system and modelled as the cardiac output Q. The cardiac output was not controlled by values in this model but was estimated using the measured heart rate. Q was estimated using the product of the measured heart rate and the stroke volume:

$$Q = HR \cdot SV \tag{17}$$

Where HR is the continuously measured heart rate and SV is the stroke volume. SV is assumed to be constant over time. Different SV values were used for male and female subjects to account for physiological variations in SV between genders [37], but a constant SV was assumed for all individuals within the same gender group. Therefore, the value was the same for all male subjects and was the same for all female subjects.

2.5 Model variations

For estimation of metabolic production, as explained in Section 2.4.5, two different approaches were utilized.

2.5.1 Model 1

The first approach used the IMU at the pelvis to estimate the kinetic energy, as this location is closest to the actual centre of mass of the participant. It was expected that this location provided a good approximation of the body's overall movement. This approach is referred to as 'model 1' and is represented by the following equation:

$$E(t) = \frac{\frac{1}{2} \cdot M_B \cdot v_{pelvis}^2(t)}{\mu} \tag{18}$$

Here, $E(t)$ represents the estimated kinetic energy at time t in kJ, M_B is the total body mass in kg, v_{pelvis} is the velocity of the pelvis in m/s, and μ is the dimensionless muscle efficiency factor.

2.5.2 Model 2

The second approach estimated the kinetic energy for the left leg, right leg, and upper body using IMUs at both thighs and the pelvis. The energies from these three body parts were summed to estimate the total kinetic energy. This approach is referred to as 'model 2'. It was expected that this approach would improve the model predictions during activities where the legs move significantly but the pelvis experiences limited movement, such as during cycling on an ergometer. The equation for Model 2 is:

$$E(t) = \frac{\frac{1}{2} \cdot \left(M_U \cdot v_{pelvis}^2(t) + \cdot M_L \cdot v_{left\_thigh}^2(t) + \cdot M_L \cdot v_{right\_thigh}^2(t) \right)}{\mu} \tag{19}$$

Where M_U represents the mass of the upper body in kg, M_L and M_R represent the mass of the left and right leg in kg, respectively. v_{pelvis}, v_{left_thigh}, and v_{right_thigh} represent

the velocity of the pelvis, left thigh, and right thigh in m/s, respectively. μ represents the dimensionless muscle efficiency factor.
The mass of each segment (e.g. M_U, M_L, and M_R) was calculated as a fraction of the total body mass. Average mass percentages for each body segment were determined by Plagenhoef *et al.* [38]. On average for men, one leg consists of 16.68% of the total weight and the remaining part of the body consists of 66.64% of the total weight. For women, one leg consists of 18.43% of the total weight and the rest of the body consists of 63.14% of the total weight. These percentages were multiplied by the total body mass of the individual to get an estimation of the mass of the upper body, left leg, and right leg.

2.6 System solver and parameter estimation

Numerical integration was performed using the Scipy Python library [39]. The dopri5 integrator was employed, which is an explicit runge-kutta method with stepsize control. The maximum step size was set to 1 second and the number of steps was limited to 10,000 steps, ensuring a comprehensive exploration of the solution space.

The computations were performed on a PC equipped with an Intel Core i5 4570 3.2 GHz CPU, 12.0 GB dual-channel DDR3 RAM, and an NVIDIA GeForce GTX 750 Ti GPU. This setup provided sufficient computational power for the calculations required in this study.

Some parameters strongly influence the dynamics of body systems and are individual dependent, but are difficult to measure. The muscle efficiency value, denoted as μ in the mathematical model description, is a critical parameter in determining the metabolic production rate. In our model, we estimated μ using parameter estimation techniques. A leave-one-out (LOO) approach was employed for parameter estimation and model evaluation. A grid search was performed to optimize the predictive model by minimizing the root mean squared error (RMSE).

Typically, human muscle efficiency spans from 15% to 35%, reflecting the variability observed across different muscles and contraction types [40, 41]. However, the current methodology for estimating metabolic production is simplified and likely underestimates actual metabolic rates, as it only includes velocity and ignores energy expenditure from acceleration and holding posture. To address this, the permissible range for μ was broadened. 50 equally spaced values within the range of 0.1% and 5% were evaluated, aiming to minimize the difference between the actual energy expenditure and the model's predictions. This range was determined after an initial exploration of a broader set of values, which indicated that the optimal μ value fell within this narrower interval.

2.7 Model evaluation

For evaluation, we first calculated the Pearson correlation coefficient between ground truth VO_2 and the velocity and kinetic energy of each IMU to investigate the relationship between the input of the model and the ground truth. Also, the correlation coefficient between VO_2 and the kinetic energy using model 2 was estimated. The Pearson correlation coefficient was calculated as follows:

$$r = \frac{\sum(x_i - \bar{x})(y_i - \bar{y})}{\sqrt{\sum(x_i - \bar{x})^2 \sum(y_i - \bar{y})^2}} \tag{20}$$

Where r denotes the correlation coefficient, x_i denotes the value of the x variable, $\bar{x}$ denotes the mean of the x variable values, y_i denotes the value of the y variable, $\bar{y}$ denotes the mean of the y variable values.

Furthermore, the normalized velocity (v) and squared velocity (v^2) were visualized for the pelvis, right thigh and left thigh and compared to the ground truth VO_2 for participant 7. Performance over the full recording and also per activity was evaluated using the RMSE, expressed in terms of kJ/min/kg:

$$\text{RMSE} = \sqrt{\sum_{i=1}^{n} \frac{(\hat{y}_i - y_i)^2}{n}} \tag{21}$$

Where n represents the total number of values, $\hat{y}_i$ represents the ground truth PAEE in kJ/min/kg at time index i, and y_i represents the predicted PAEE in kJ/min/kg at time index i.

Furthermore, the R-squared over the full recording was calculated to evaluate the capacity of the model to capture the variations in energy expenditure due to different activities:

$$R^2 = 1 - \frac{\sum_i (y_i - \hat{y}_i)^2}{\sum_i (y_i - \bar{y})^2} \tag{22}$$

Where n represents the total number of values, y_i represents the predicted PAEE in kJ/min/kg at time index i, $\hat{y}_i$ represents the ground truth PAEE in kJ/min/kg on time index i, and $\bar{y}$ represents the mean of the ground truth PAEE values. When the numerator is greater than the denominator, meaning that the model performs worse than the average line, the R^2 will be negative.

The predicted energy expenditure was plotted for the participant with the highest R^2 for both models and compared to the ground truth to visualize the differences between the models.
Consequently, we analyzed the effect of a preceding activity on the RMSE of the successive activity. This was done by grouping all activities by their preceding activity type, e.g. LWBM denotes activities whose preceding activity type is LWBM. Then, we employed a t-test to compare the RMSE values of these grouped activities.

Finally, we investigated the effect of the assumption of a constant RQ on the error of the model, as the RQ significantly impacts the quality of the model's input. Our model utilizes R_{M,O_2} and R_{M,CO_2} as input, making the accuracy of these values crucial for the model's performance. According to Equation 15, R_{M,CO_2} is the product of RQ and R_{M,O_2}, which is the part where the error would be introduced. Normally, the RQ is individual-dependent and activity-dependent, so the value of the RQ changes with every time step. However, with a constant RQ, there will be an error in the estimation of R_{M,CO_2} even when R_{M,O_2} is estimated without any error. For this analysis, we assumed a perfect model except for the value of RQ. This was done by setting the R_{M,O_2} equal to the ground truth VO_2. Using this, the R_{M,CO_2} was estimated using a constant RQ and energy expenditure was estimated using Weir's formula accordingly, which is mentioned in Equation 12. This predicted energy expenditure was then compared to the ground truth energy expenditure using the RMSE metric. As the model was assumed to be perfect, all errors in terms of RMSE can be assigned to the assumption of the constant RQ. The results of this analysis are presented

as the error percentage between the RMSE from the so-called 'perfect model', as described in this paragraph, and the RMSE from either model 1 or model 2. This was done to clearly show the magnitude of the error originating in the constant RQ assumption in comparison to the predictions of the regular models. The error percentage was calculated using the following equation:

$$\text{error} = 1 - \frac{\left|\varepsilon_{RQ} - \varepsilon_{model_j}\right|}{\varepsilon_{model_j}} \tag{23}$$

Where the error denotes the contribution of the constant RQ on the total RMSE of the models. ε_{RQ} represents the error of the so-called 'perfect model' in RMSE, ε_{model_j} represents the error of the models described in Section 2.5 in RMSE, where j represents the model approach number.

3 Results

We initially recruited 7 men and 3 women to participate in the experiment. The data of participant 4 (male) was unusable due to disconnected sensors, so this participant was excluded. The demographic information of the nine remaining participants is shown in Table 2. Notably, the data reveals a lower average weight and muscle percentage among the female participants, compared to the male participants. The table highlights the diversity in body composition within the group, as reflected by the range of BMI, muscle percentage, and fat percentage values.

Table 2: Main demographics of the study population. Rest metabolic rate (RMR) was calculated using the Weir equation [34].

Participant	Sex	Age (years)	Weight (kg)	Height (cm)	BMI (kg/m^2)	RMR (kcal)	Muscle (%)	Fat (%)
1	Female	23	54.6	170	18.9	2154	31	24.1
2	Male	24	83.5	187	23.9	2124	41	17
3	Male	23	84.5	175	27.6	2307	35.7	28
5	Male	49	70.7	186	20.4	1945	36.3	18
6	Male	29	92.2	178	29.1	2364	34.1	29.5
7	Female	23	65.5	177	20.9	1923	28.9	30.4
8	Male	23	73.4	183	21.9	2247	41	17.3
9	Male	23	77.2	187	22.1	3259	38.3	21
10	Female	23	61.9	169.5	21.5	1423	26	34.3

3.1 Correlation analysis

The Pearson correlation coefficient between the measured VO_2 and both velocity and kinetic energy was calculated. The mean and standard deviation of the correlation coefficient are shown in Table 3. For all locations, the kinetic energy has a weaker correlation with VO_2 compared to the velocity. Both the right and left thighs have the highest mean correlation coefficients with VO_2 for both velocity and kinetic energy, while the wrists show the lowest correlation coefficients. Generally, the lower body locations (thighs and dominant shoe) have higher correlation coefficients compared to the upper body locations (shoulders, sternum, chest). The velocity and squared velocity of the IMU on the pelvis, right thigh, and left thigh are plotted with the ground truth VO_2 in Figure 5. For each location, the squared velocity shows a decreased value compared to the velocity. As the velocity is smaller than 1 m/s at most timestamps, the quadratic relationship returns a decrease in the squared velocity compared to the velocity. It can be observed that the thigh IMUs capture more movement during the cycling and walking activities, compared to the pelvis IMU. However, the ground truth VO_2 shows a larger relative increase during cycling than the IMUs can capture in terms of velocity.

In light of the model's required explainability, the primary focus is placed on the estimated kinetic energy. A notable correlation exists between kinetic energy and VO_2 for the thighs, indicating potential enhancements through the addition of the IMUs on the thighs. The mean and standard deviation of the correlation coefficient between VO_2 and the weighted average of the left thigh, right thigh and pelvis are 0.559 and ± 0.162, respectively. Given that this correlation is stronger than that of using only the pelvis IMU, both approaches were analysed.

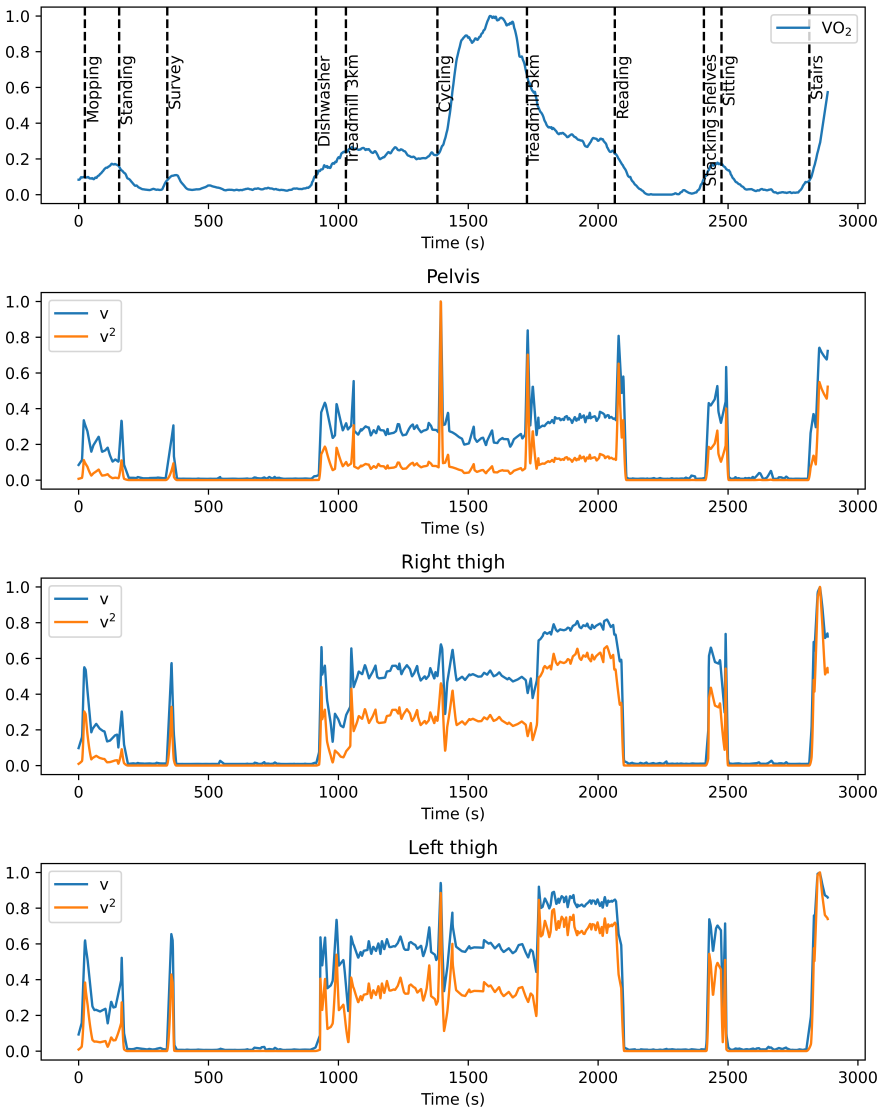

Figure 5: Normalized VO_2 and normalized velocity (v) and v^2 of the IMUs located at the pelvis, right thigh, and left thigh on participant 7.

Table 3: Pearson correlation coefficient between VO_2 and velocity of IMU, and between VO_2 and kinetic energy.

IMU location	VO_2 and velocity	VO_2 and kinetic energy
Left shoulder	0.437 ± 0.141	0.305 ± 0.131
Right shoulder	0.419 ± 0.180	0.310 ± 0.158
Sternum	0.468 ± 0.136	0.316 ± 0.131
Chest	0.446 ± 0.141	0.255 ± 0.213
Left wrist	0.311 ± 0.196	0.272 ± 0.191
Right wrist	0.265 ± 0.191	0.227 ± 0.177
Pelvis	0.478 ± 0.152	0.350 ± 0.157
Right thigh	0.697 ± 0.115	0.627 ± 0.152
Left thigh	0.654 ± 0.156	0.571 ± 0.199
Shoe (dominant leg)	0.539 ± 0.148	0.417 ± 0.176

3.2 Model performance

On average, the model's numerical integration took approximately 0.48 seconds, with a standard deviation of 0.12 seconds. Considering 9 participants, 50 sets of parameters, and 2 models, this integration process was performed a total of 7218 times. When examining the estimated muscle efficiency values, model 1 had a median value of 0.013 and an interquartile range of 0.011. Model 2 exhibited a higher median muscle efficiency value of 0.028, with an interquartile range of 0.018. This suggests that the approach of model 2 utilizing multiple IMUs provides a more precise approximation of the input magnitude as the model input is scaled using the muscle efficiency value.

To assess performance, the aggregate R^2 and RMSE values for the complete dataset for each participant are shown in Table 4. Furthermore, a detailed analysis of the RMSE for individual activities per model is presented in Table 5. More detailed results per participant are presented in Section A.2 in the appendix, in which Table 9 contains the RMSE for each activity per participant utilizing Model 1, which relies solely on the kinetic energy from the pelvis IMU, and Table 10 contains the RMSE values for the same activities using Model 2, which incorporates a weighted average of the thighs and pelvis.

Model 1 exhibits a significantly lower mean R^2 compared to model 2 (0.256 ± 0.302 vs. 0.375 ± 0.312, p=0.05). Regarding the overall RMSE, model 1 demonstrates a similar mean value compared to model 2 (0.112 ± 0.035 vs. 0.100 ± 0.037, p = 0.08). Moreover, participants 1, 2, 6, and 7 show a higher R^2 for model 1 compared to model 2. In addition, participants 1, 2, and 7 have a smaller RMSE for model 1 compared to model 2, indicating that model 1 performs better for these participants. The results indicate a considerable variability among individuals. Notably, both models yield a negative R^2 for participant 10. Above all, participant 6 exhibits superior performance for model 2 compared to the other predictions, showing an R^2 value of 0.734.

In terms of the mean RMSE per activity, cycling and standing exhibit the largest mean RMSE values for both models. No significant difference was found in the performance of model 1 and model 2 for any of the activities. When examining the sedentary activities of standing and sitting, which involve minimal to no movement, a distinction can be found. The RMSE of model 1 is significantly higher for standing compared to sitting (0.116 ± 0.050 vs. 0.055 ± 0.020, $p < 0.01$). No significant difference was found between these

activities for model 2 (0.103 ± 0.051 vs. 0.057 ± 0.034, p = 0.06).

Table 4: The aggregate R^2 and RMSE (kJ/min/kg) of the predictions using either model 1 or model 2.

	Model 1		Model 2	
Participant	Overall R^2	Overall RMSE	Overall R^2	Overall RMSE
1	0.197	0.166	0.126	0.173
2	0.634	0.049	0.532	0.056
3	0.005	0.099	0.197	0.089
5	0.529	0.102	0.705	0.081
6	0.583	0.070	0.768	0.052
7	0.385	0.104	0.381	0.105
8	0.335	0.139	0.734	0.088
9	-0.068	0.127	0.098	0.116
10	-0.296	0.148	-0.162	0.141
Mean±std	0.256±0.302	0.112±0.035	0.375±0.312	0.100±0.037

Table 5: Mean and standard deviation of RMSE (kJ/min/kg) for each activity using either model 1 or model 2.

Activity	Model 1	Model 2
Treadmill 3 km/h	0.048 ± 0.027	0.057 ± 0.029
Treadmill 5 km/h	0.054 ± 0.027	0.069 ± 0.027
Cycling	0.255 ± 0.107	0.213 ± 0.115
Stacking shelves	0.079 ± 0.059	0.061 ± 0.027
Standing	0.116 ± 0.050	0.103 ± 0.051
Sitting	0.055 ± 0.020	0.057 ± 0.034
Reading	0.068 ± 0.036	0.059 ± 0.037
Dishwasher	0.069 ± 0.034	0.057 ± 0.030
Stairs	0.058 ± 0.031	0.064 ± 0.034
Mopping	0.071 ± 0.042	0.064 ± 0.030
Survey	0.065 ± 0.052	0.054 ± 0.037

The predictions by both models on the data of participant 6 are shown in Figure 6. Both models overestimate most of the activities, except for the cycling activity, which is underestimated. Model 1 shows a very fast response to the HWBM activities, which include emptying the dishwasher, mopping, and stacking books, but overshoots the ground truth value. After the HWBM activities and walking at 5 km/h activity, the model responded very slowly, resulting in an overestimated prediction. Similar to model 1, model 2 has a slow response after walking at 5 km/h activity, which results in an overestimation. However, the spikes at the beginning of the reading and dishwasher activity for model 1 are not visible in model 2. The predictions for all participants are visualized in the appendix in Section A.3.

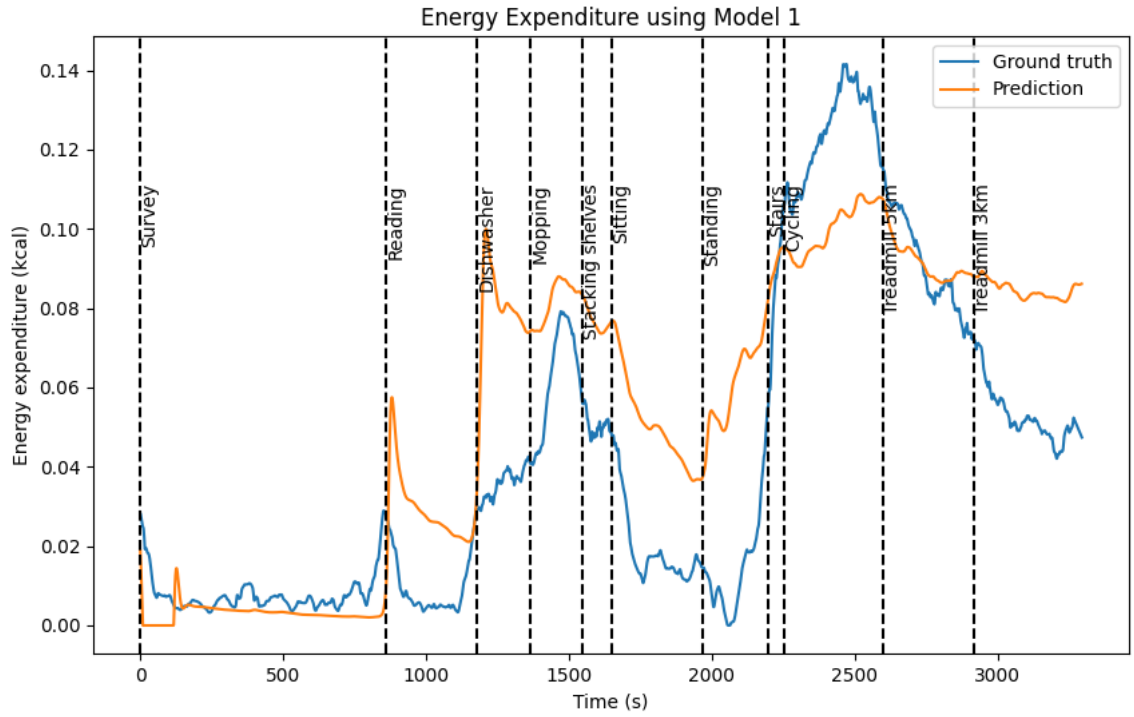

(a) Ground truth and predicted PAEE using model 1.

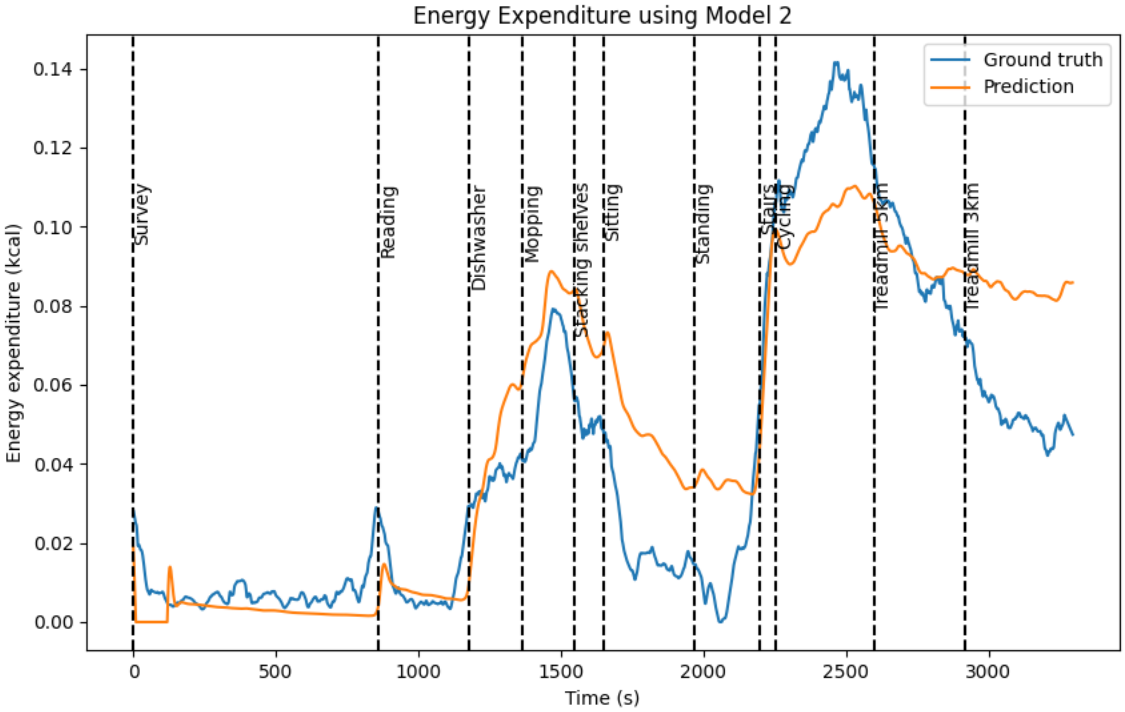

(b) Ground truth and predicted PAEE using model 2.

Figure 6: Comparative PAEE predictions for participant 6 using the two different models.

3.3 Introduced error by constant RQ

Table 6 presents a comparison of the percentage of error induced by the assumption of constant RQ in the two different predictive models across the participants. The error percentages per model represent the contribution of the constant RQ on the total RMSE of the models from Table 4. It can be observed that the error percentages for model 1 and model 2 are relatively close across participants. The smallest error percentages are observed at participant 10 (2.9% for model 1 and 3.1% for model 2). The largest percentage for model 1 is observed in participant 2 at 6.9%, and the largest percentage for model 2 is observed in participant 6 at 8.0%. This analysis indicates that the assumption of constant RQ introduces approximately between 2.9% and 8.0% of the total error.

Table 6: Percentage of error induced by constant RQ in predictive models.

Participant	Model 1 RQ Error (%)	Model 2 RQ Error (%)
1	5.8	5.5
2	6.9	6.1
3	3.6	3.9
5	5.3	6.7
6	5.9	8.0
7	6.0	6.0
8	4.8	7.6
9	3.0	3.3
10	2.9	3.1

3.4 Effect of preceding activity

The results of pairwise comparisons between RMSE values, grouped by preceding activity type (LWBM, HWBM, walking, and cycling), are presented in Table 7. The LWBM group, consisting of RMSE values of activities that had an LWBM activity as preceding activity, showed a significantly lower RMSE on average in kJ/min/kg compared to the other groups combined for both model 1 (0.062 vs 0.093, p=0.02) and model 2 (0.055 vs 0.086, p <0.01). The other groups did not show a significant difference compared to the other groups.

Table 7: Student's t-test p-values for pairwise comparisons between RMSE values of one group and all others combined. The groups consist of low whole-body motion (LWBM) activities, high whole-body motion (HWBM) activities, walking activities, and cycling. Asterisks denote the level of significance, where one asterisk (*) indicates $p < 0.05$.

Group	n	p-value (Model 1)	p-value (Model 2)
LWBM	31	0.02*	< 0.01*
HWBM	25	0.64	0.98
Walking	20	0.21	0.07
Cycling	8	0.68	0.72

4 Discussion

In this thesis, we introduced a novel approach for PAEE estimation by combining a physiological model and sensor data within a simplified physiological computing model. Our method stands out by integrating real-time sensor data measurements with a physiological understanding of the dynamics of energy expenditure, offering a more detailed and personalized framework compared to traditional methods. By employing the power of both domains, we provide a tool that opens new avenues for energy expenditure modelling techniques.

4.1 Discussion and interpretation of results

The correlation analysis revealed that the predictive power of velocity and kinetic energy varies with the placement of the IMU. Notably, the lower body locations, specifically the thighs, demonstrate higher mean correlation coefficients with VO_2. This suggests that movement in the lower body is more reflective of VO_2 levels, which is consistent with the understanding that the lower body is typically more involved in activities that elevate VO_2. The pelvis showed a weaker predictive relationship, likely because it experiences minimal movement during treadmill and ergometer exercises. The thighs capture significant movement during walking and cycling activities. The significant movement observed in the thighs during walking and cycling activities accounts for the notably stronger correlation observed between the velocity and kinetic energy at this location and VO_2.

Model 1 exhibited a significantly lower mean R^2 compared to model 2 (0.256 ± 0.302 vs. 0.375 ± 0.312, p=0.05), even though model 1 shows a higher R^2 for four subjects. Regarding the overall RMSE, model 1 demonstrated a similar mean value compared to model 2 (0.112 ± 0.035 vs. 0.100 ± 0.037, $p = 0.08$). The performance difference is presumably caused by the inclusion of the thigh IMUs, as this makes the model less dependent on the movement of one single body component. The stronger correlation between VO_2 and the weighted average of the left thigh, right thigh, and pelvis compared to using only the pelvis IMU, in addition to the improved predictions, supports the use of a multi-sensor approach over a single-sensor model.

In the evaluation of the models, it is important to consider both quantitative and qualitative aspects. While the R^2 shows relatively poor performance, the figures in Section A.3 demonstrate that the model captures the changes in PAEE quite well by following the trends in the ground truth PAEE values. The R^2 may not always be the most appropriate metric for evaluating how well the model captures the underlying pattern, or variance, in PAEE. This is because R^2 measures the proportion of explained variance rather than the magnitude of the prediction error. Therefore, a model could have a low R^2 but still make predictions that are close to the ground truth values. This is especially the case if the scale of the output is small. For this study, we used RMSE and R^2 to facilitate comparison with other studies. However, we recognize the limitations of these evaluation metrics on this application.

In the appendix in Section A.3, it can be observed that the model predictions have a large variation between participants. The quantitative metrics do not match with the qualitative analysis of the predictions for all participants, as mentioned in the previous paragraph. For example, participant 10 exhibits poor R^2, while the predicted graph does follow the trend of the ground truth PAEE quite well. We recognize the variations in predictions, but it ap-

pears difficult to suggest a clear explanation for each individual. Overall, the origin of the variations in performance probably lies in the physiological differences between individuals and how each participant approached the activities. However, we might be able to explain the enhanced performance of both models in the case of participant 6. This participant chose to cycle with a low cadence, leading to a comparatively lower PAEE during cycling, which contrasts with the higher expenditures of other participants. Typically, the models tend to underestimate PAEE during cycling as the resistance of the bike is not reflected in the IMU data. However, due to the slower cycling pace by participant 6, the performance of both models for this participant improved. This is supported by the data presented in Table 9 and Table 10, where the RMSE for cycling by participant 6 is nearly half of the RMSE for the other participants during the same activity.

The analysis of the impact of the preceding activity on the accuracy of PAEE estimation provides valuable insights into the dynamics of PAEE and the influence on predictive modelling. The findings suggest that preceding LWBM activities significantly affect the estimation performance of consequent activities in terms of RMSE, as activities with preceding LWBM activities exhibit significantly lower RMSE values compared to other preceding activities. In other words, the characteristics of LWBM activities may lead to physiological changes that impact subsequent metabolic rates. For example, engaging in sedentary activities results in a more stable and predictable metabolic rate and physical state. Because of this, the energy expenditure might be easier to predict when transitioning to a more active task. This contrasts with transitions from more variable activities, such as HWBM or walking, where the abrupt changes in metabolic rate can introduce greater variability and challenging predictions. Thus, the more stable and predictable transition from LWBM activities may lead to better model performance.

It can be observed that both models have difficulties in estimating the change in PAEE in between activities. This could be caused by the simplified control system, as it only includes a linear dependency on arterial O^2 concentration and alveolar CO_2 pressure. It could also be caused by the simplified approach for estimating metabolic production using kinetic energy, as changes in kinetic energy might not fully capture the required muscle contractions for posture and activity changes. This is supported by the significant difference in RMSE between the sitting and standing activity. Even though both activities involve minimal to no movement, the actual energy expenditure differs due to the required muscle contractions for holding posture. The model estimates a similar PAEE for both activities due to the similar movement intensity, resulting in a significantly larger RMSE for the standing activity.

4.2 Comparative evaluation with existing literature

In comparing our findings with those of Heil *et al.* [42], who reported an R^2 of 0.71 using a hip-mounted IMU, our study achieved a lower R^2 of 0.375. This difference may be attributed to our use of 1-second epochs, which provide a more specific view of PAEE but also introduce greater variability in the data, compared to their 60-second epochs. In addition, Heil *et al.* did not account for time dynamics between activities by treating each epoch as an independent data point, which could lead to errors in short periods with large variations in activity type.

Similarly, Bouten *et al.* found a strong relationship between the accelerometer output and

PAEE (r=0.95). Their equation underestimated individual PAEE during sitting, writing and arm work by 35-140%, while sitting down/standing up was overestimated by 70%. These findings are in agreement with our findings, showing the difficulty of estimating energy expenditure during sedentary activities and transitions between activities. They found that the forward direction of acceleration intensity was a better predictor of PAEE than the upward direction during walking, running and stepping exercises. Importantly, they did not find a clear relationship between PAEE and kinetic energy calculated using the velocity of the lower back, which is in agreement with our findings that the velocity has a stronger correlation with VO_2 than kinetic energy with VO_2.

Van Hees *et al.* estimated PAEE in participants for 23 hours in a respiration chamber while performing a set of activities such as walking, standing, sitting and lying [43]. Using an accelerometer at the lower back and a best-fit linear equation, the activity type was derived. Using an equation for each activity type, the PAEE was predicted for each individual using 30-minute averages, achieving an R^2 with PAEE of 0.81 ± 0.06. The superior performance of their approach compared to ours could be explained by their small number of activity types and the 30-minute epochs, which neglects the need for accurately estimating the transitions between activities. However, this approach underscores the need for activity type derivation in the model.

4.3 Contribution to the field

The inferior performance of our model compared to published models does not diminish the contribution of this research to the field of PAEE and obesity prevention. Firstly, we have collected a diverse dataset consisting of a large number of sensors. This dataset is more realistic and contains limited bias when compared to published datasets, mainly due to the variation of ADL and the randomized order of the activities. This, in combination with the relatively high sampling frequency, allows for a realistic evaluation of the model. It is expected that models which are evaluated on a more realistic dataset give worse results compared to a less realistic dataset. Nevertheless, training and evaluation using our dataset would represent real-life performance, which is after all essential for effective interventions for obesity prevention.

Secondly, to our best knowledge, we are the first to include dynamics into a PAEE estimation model. An explainable and thus physiological and dynamic model is essential as PAEE has a high inter-individual variation. Our model allows the insertion of measurable individual-specific parameters, such as muscle mass percentage and weight, which are implemented in the model using physiological knowledge. Also, more complex parameters, for example, the ones in the ventilatory control system, could be trained within a physiologically realistic range to make the model personalized while keeping it explainable. Additionally, in comparison to a black box model approach, our simplified and computationally efficient approach ensures that the model can easily adapted and scaled for real-world applications. Because of the explainable and personalized characteristics of the model, this approach allows to transcend current existing models that are being used for PAEE estimation. In the end, personalized estimations of energy expenditure are needed to reduce the gap between consumed energy and expended energy.

4.4 Limitations and recommendations

While the assumptions and simplifications made in this study are essential to make the project manageable, it is important to recognize their limitations. These simplifications may affect the performance of the model in terms of generalizability and could introduce certain biases. Specifically, the assumption of constant RQ overlooks the complex interplay of different energy systems in the body. As discussed in Section 3.3, the constant RQ introduces approximately between 2.9% and 8.0% of the RMSE when the estimated VO_2 equals the ground truth. However, it could be hypothesized that the error percentage increases when the error between the estimated and ground truth VO_2 decreases. In addition, the number of estimated parameters was set to one due to limited time and computational power. It is recommended to estimate more parameters to make the model more personalized. In addition, the leave-one-out approach is not optimal for tailoring the model as parameters are not optimized on the leave-one-out participant, but on the remaining group of participants. For future research, it is recommended to start each measurement with a series of fixed activities which could be used for within-subjects parameter estimation.

For the breath-by-breath analyser, three calibration steps needed to be performed. One of the calibration steps was performed using a gas tank with known concentrations of O_2 and CO_2 to make sure that the analyser measured the air concentrations correctly. Unfortunately, we were not able to perform the concentration calibration before each measurement day, given the current regulations on storing gas tanks. Due to this, we performed this calibration step once a week which could have introduced errors in the ground truth data. It is unknown whether the limited calibration results in an under- or overestimation of energy expenditure. For the future, it is recommended to perform all calibration steps on every measurement day to ensure correct ground truth data.

Currently, the metabolic production estimation is explainable but also extremely simplified. The current approach assumes no metabolic production when there is movement. This ignores the energy expenditure of holding posture, which differs significantly between standing and sitting positions. Francisco *et al.* found the mean difference in PAEE between standing and sitting positions to be significant (0.52 ± 1.01 kJ/min, $P<0.001$) [44], which could explain the inferior performance for standing activity compared to sitting activities. For future research, it is recommended to improve the metabolic production estimation by incorporating energy expenditure caused by holding posture. The use of activity classifiers for ADL, as already done with high accuracy by several studies [45, 46, 47], could be a useful approach to determine PAEE for different activities with corresponding postures.

In addition, our approach neglects the direction of the movement by using the magnitude of the velocity vector. According to the findings of Bouten *et al.*, it is recommended for future research to make a distinction between forward and upward movement. According to the findings of Van Hees *et al.*, making the model dependent on the activity type might enhance the performance. This could be done by determining an efficiency factor for each activity separately to further improve the estimation of metabolic production.

5 Conclusion

In this thesis, we presented an innovative approach for PAEE estimation by integrating physiological models with sensor data in a simplified physiological computing model. The proposed method demonstrates the potential to provide more detailed and personalized PAEE estimations during ADL compared to traditional models. Through the integration of real-time sensor data in a physiological dynamic system, this research has made strides towards future advancements in terms of the accuracy and usability of PAEE estimators. This approach shows the potential to play a role in addressing the global obesity pandemic by enabling individuals to better understand and manage their energy expenditure.

A Appendix

A.1 Glossary table

Table 8: Glossary of used symbols. *subject-specific* represents subject-specific values, which were measured or estimated for each individual. All used values were taken from [30], except values for K_2, K_3, K_4, ρ, SV_m, and SV_f.

Symbol	Subscript	Species	Definition	Unit	Basal value
C			[Concentration]	L / L	
	a	O_2	Arterial		0.192
		CO_2			0.572
	e	O_2	End-capillary		0.193
		CO_2			0.570
	T	O_2	Muscle tissue		$13.0 \cdot 10^{-4}$
		CO_2			0.605
	v	O_2	Venous		0.144
		CO_2			0.610
P			[Partial pressure]	$mmHg$	
	A	O_2	Alveolar		100.2
		CO_2			40.28
	I	O_2	Inspired air [48]		160
		CO_2			0.3
p_s			Pulmonary shunt fraction		0.024
λ			Conversion coefficient	$mmHg$	863
$\dot{V}$			[Ventilation]	L/s	
	0		Basal value		0.0713
	A		Alveolar		0.0713
G			[Peripheral gain]		
	p, O_2			$L \cdot s^{-1}$	2.45
	p, CO_2			$L \cdot s^{-1} \cdot mmHg^{-1}$	0.0316
K					
	1				-0.783
	2		Oxygen [31]	$(mmHg)^{-1}$	0.2
	3		Oxygen [31]	$(mmHg)^{-1}$	0.046
	4		Carbon dioxide [31]		0.016
V			[Volume]	L	
	A		Alveolar		3.28
	T		Tissue		38.74
ρ			Skeletal muscle density [49]	kg/dm^3	1.06
R	M		[Metabolic production rate]		
		O_2		L/s	0
		CO_2			0
SV			[Stroke volume] [37]	L	
	m		Male		0.08975
	f		Female		0.06932
v			Velocity	m/s	0
E			Energy	J	0
HR			Heart rate	$beats/min$	*subject-specific*
Q			Cardiac output	L/s	*subject-specific*
M			[Mass]	kg	
	B		Body		*subject-specific*
	SM		Skeletal muscle		*subject-specific*
	U		Upper body		*subject-specific*
	L		Leg		*subject-specific*
μ			Human muscle efficiency	%	*subject-specific*

A.2 Performance of models per participant per activity

Table 9: RMSE (kJ/min/kg) per participant for each activity using model 1.

Participant	Treadmill 3 km/h	Treadmill 5 km/h	Cycling	Stacking shelves	Standing	Sitting	Reading	Dishwasher	Stairs	Mopping	Survey
1	0.071	0.076	0.369	-	0.146	0.061	-	0.109	0.067	-	-
2	0.019	-	-	0.044	-	0.019	0.024	0.058	0.108	0.089	0.058
3	0.028	0.032	0.259	0.024	0.075	0.063	0.091	0.085	0.026	0.031	0.031
5	0.093	0.058	0.122	0.076	0.157	0.043	0.101	0.041	0.086	0.079	0.137
6	0.087	0.022	0.069	0.072	0.127	0.087	0.058	0.124	0.034	0.057	0.019
7	0.021	0.063	0.261	0.022	0.013	0.053	0.116	0.040	0.056	0.042	0.012
8	0.043	0.027	0.341	0.216	0.085	0.056	0.039	0.057	0.019	0.088	0.093
9	0.043	0.046	0.229	0.113	0.173	0.081	0.099	0.091	0.028	0.161	0.152
10	0.024	0.109	0.389	0.069	0.148	0.031	0.017	0.014	0.095	0.020	0.021
Mean	0.048	0.054	0.255	0.079	0.116	0.055	0.068	0.069	0.058	0.071	0.065
Std	0.027	0.027	0.107	0.059	0.050	0.020	0.036	0.034	0.031	0.042	0.052

Table 10: RMSE (kJ/min/kg) per participant for each activity using model 2.

Participant	Treadmill 3 km/h	Treadmill 5 km/h	Cycling	Stacking shelves	Standing	Sitting	Reading	Dishwasher	Stairs	Mopping	Survey
1	0.079	0.072	0.398	-	0.104	0.047	-	0.080	0.095	-	-
2	0.038	-	-	0.037	-	0.024	0.023	0.073	0.111	0.103	0.058
3	0.029	0.068	0.208	0.039	0.065	0.063	0.098	0.121	0.024	0.030	0.025
5	0.092	0.035	0.110	0.075	0.130	0.021	0.084	0.042	0.087	0.078	0.077
6	0.087	0.023	0.064	0.063	0.066	0.080	0.019	0.038	0.027	0.047	0.021
7	0.034	0.091	0.255	0.022	0.014	0.030	0.113	0.058	0.084	0.037	0.014
8	0.051	0.108	0.105	0.114	0.119	0.121	0.033	0.021	0.021	0.075	0.086
9	0.093	0.065	0.194	0.074	0.191	0.100	0.083	0.061	0.036	0.109	0.126
10	0.010	0.095	0.371	0.070	0.137	0.030	0.017	0.019	0.089	0.031	0.029
Mean	0.057	0.069	0.213	0.061	0.103	0.057	0.059	0.057	0.064	0.064	0.054
Std	0.029	0.027	0.115	0.027	0.051	0.034	0.037	0.030	0.034	0.030	0.037

A.3 Predictions of the models for each participant

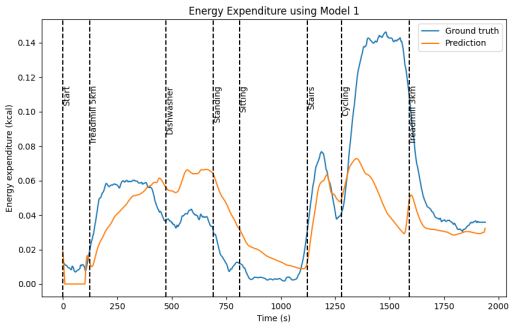

(a) Participant 1, model 1.

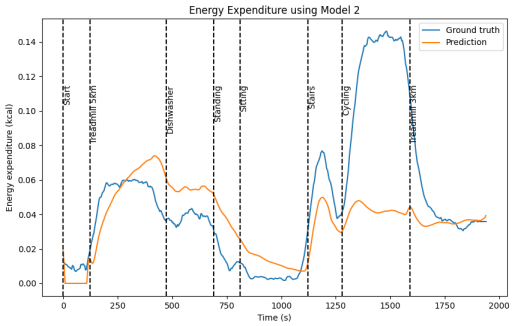

(b) Participant 1, model 2.

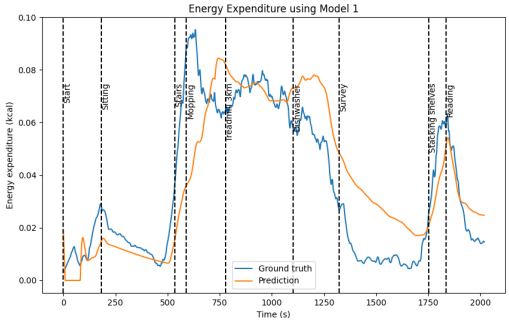

(c) Participant 2, model 1.

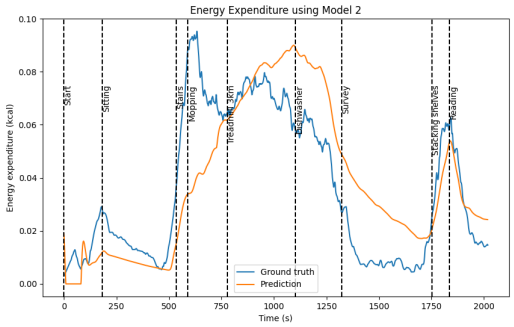

(d) Participant 2, model 2.

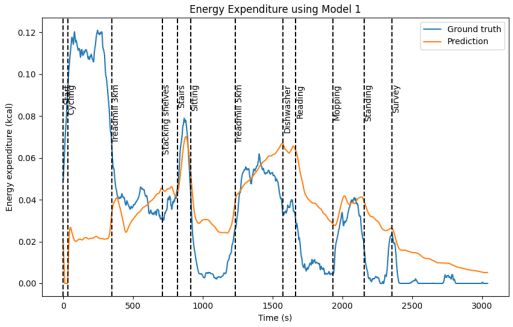

(e) Participant 3, model 1.

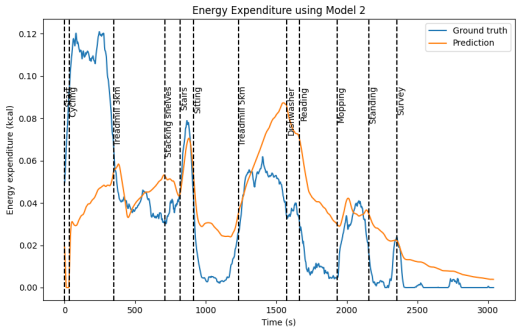

(f) Participant 3, model 2.

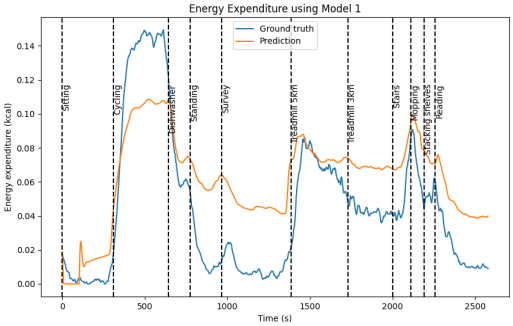

(g) Participant 5, model 1.

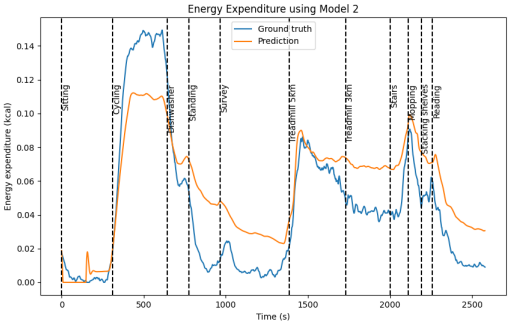

(h) Participant 5, model 2.

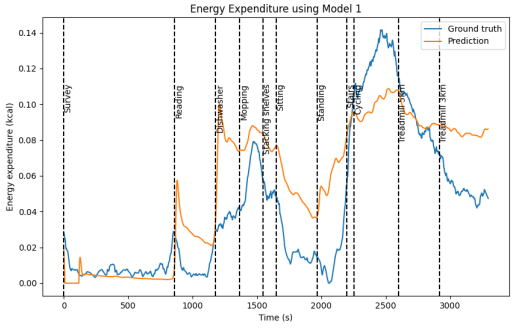

(i) Participant 6, model 1.

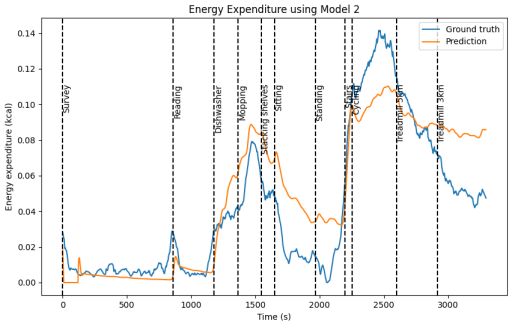

(j) Participant 6, model 2.

Figure 7: Predictions for participant 1 up to 6 using either model 1 or 2.

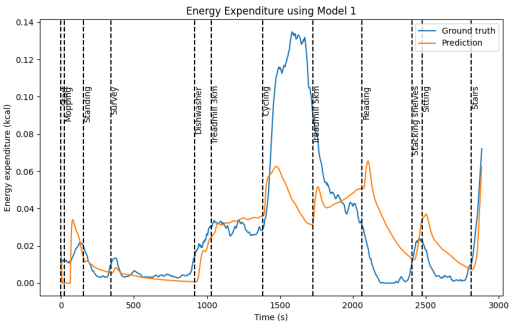

(a) Participant 7, model 1.

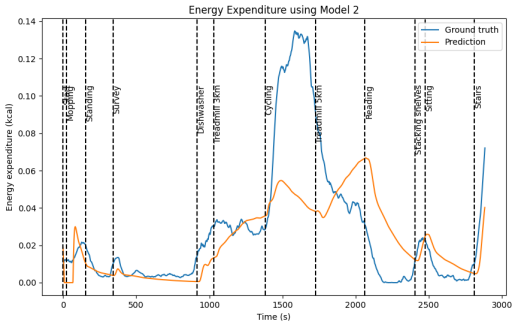

(b) Participant 7, model 2.

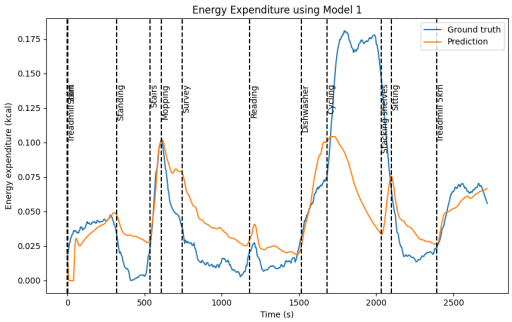

(c) Participant 8, model 1.

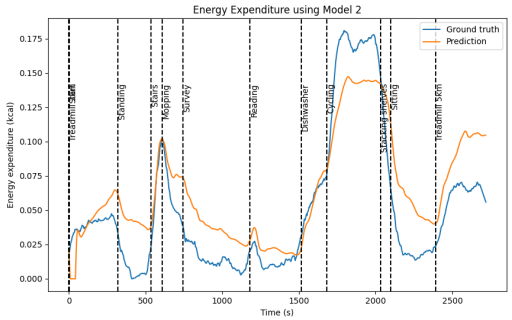

(d) Participant 8, model 2.

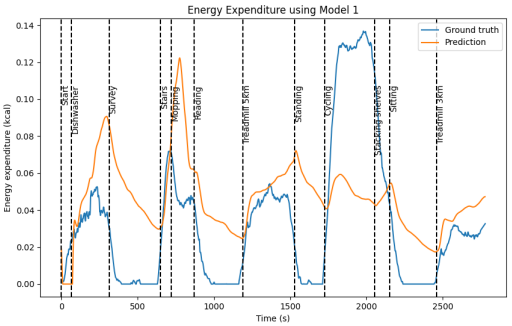

(e) Participant 9, model 1.

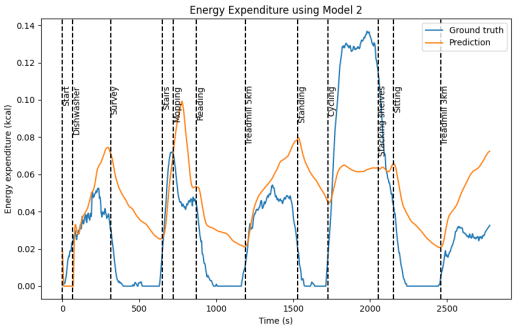

(f) Participant 9, model 2.

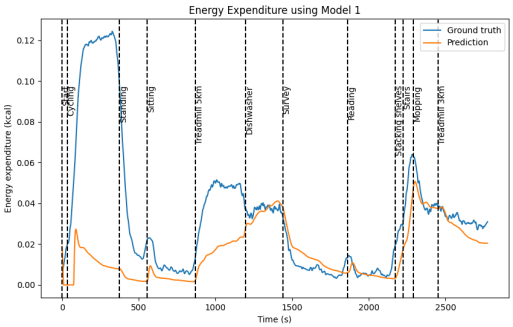

(g) Participant 10, model 1.

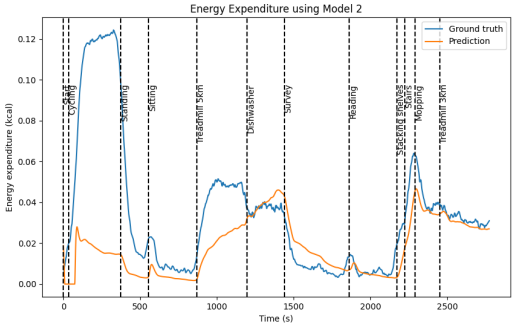

(h) Participant 10, model 2.

Figure 8: Predictions for participant 7 up to 10 using either model 1 or 2.

A.4 Order of activities per participant

Table 11: Order of activities per participant

Participant 1	**Participant 2**	**Participant 3**	**Participant 4**	**Participant 5**
Stacking shelves with books	Sitting resting	Cycling	Working on a laptop	Sitting resting
Mopping	Climbing stairs	Treadmill (3 km/h)	Sitting resting	Cycling
Standing still	Mopping	Stacking shelves with books	Standing still	Emptying dishwasher
Working on a laptop	Treadmill (5 km/h)	Climbing stairs	Treadmill (5 km/h)	Standing still
Sitting reading	Emptying dishwasher	Sitting resting	Stacking shelves with books	Working on a laptop
Treadmill (5 km/h)	Working on a laptop	Treadmill (5 km/h)	Cycling	Treadmill (5 km/h)
Emptying dishwasher	Stacking shelves with books	Emptying dishwasher	Emptying dishwasher	Treadmill (3 km/h)
Sitting resting	Sitting reading	Sitting reading	Climbing stairs	Climbing stairs
Climbing stairs	Cycling	Mopping	Sitting reading	Mopping
Cycling	Standing still	Standing still	Mopping	Stacking shelves with books
Treadmill (3 km/h)	Treadmill (3 km/h)	Working on a laptop	Treadmill (3 km/h)	Sitting reading

Participant 6	**Participant 7**	**Participant 8**	**Participant 9**	**Participant 10**
Working on a laptop	Mopping	Treadmill (3 km/h)	Emptying dishwasher	Cycling
Sitting reading	Standing still	Standing still	Working on a laptop	Standing still
Emptying dishwasher	Working on a laptop	Climbing stairs	Climbing stairs	Sitting resting
Mopping	Emptying dishwasher	Mopping	Mopping	Treadmill (5 km/h)
Stacking shelves with books	Treadmill (3 km/h)	Working on a laptop	Sitting reading	Emptying dishwasher
Sitting resting	Cycling	Sitting reading	Treadmill (5 km/h)	Working on a laptop
Standing still	Treadmil (5 km/h)	Emptying dishwasher	Standing still	Sitting reading
Climbing stairs	Sitting reading	Cycling	Cycling	Stacking shelves with books
Cycling	Stacking shelves with books	Stacking shelves with books	Stacking shelves with books	Climbing stairs
Treadmill (5 km/h)	Sitting resting	Sitting resting	Sitting resting	Mopping
Treadmill (3 km/h)	Climbing stairs	Treadmill (5 km/h)	Treadmill (3 km/h)	Treadmill (3 km/h)

References

[1] Lobstein T, Jackson-Leach R, Powis J, Brinsden H, Gray M. World Obesity Atlas 2023. World Obesity Federation; 2023. Available from: https://s3-eu-west-1.amazonaws.com/wof-files/World_Obesity_Atlas_2023_Report.pdf.

[2] World Health Organization. Obesity and overweight; 2021. Available from: https://www.who.int/news-room/fact-sheets/detail/obesity-and-overweight.

[3] de Mello Meirelles C, Chagas Gomes PS. Acute effects of resistance exercise on energy expenditure: Revisiting the impact of the training variables. Revista Brasileira de Medicina do Esporte. 2004;10(2):131-8.

[4] Hills AP, Mokhtar N, Byrne NM. Assessment of Physical Activity and Energy Expenditure: An Overview of Objective Measures; 2014.

[5] Jeran S, Steinbrecher A, Haas V, Mähler A, Boschmann M, Westerterp KR, et al. Prediction of activity-related energy expenditure under free-living conditions using accelerometer-derived physical activity. Scientific Reports. 2022 10;12(1):1-11.

[6] Speakman J, Pontzer H, Rood J, Sagayama H, Schoeller D, Westerterp K, et al. The International Atomic Energy Agency International Doubly Labelled Water Database: Aims, Scope and Procedures. Annals of Nutrition and Metabolism. 2019 12;75:114-8.

[7] Hedegaard M, Anvari-Moghaddam A, Jensen BK, Jensen CB, Pedersen MK, Samani A. Prediction of energy expenditure during activities of daily living by a wearable set of inertial sensors. Medical Engineering and Physics. 2020;75:13-22.

[8] Jeran S, Steinbrecher A, Pischon T. Prediction of activity-related energy expenditure using accelerometer-derived physical activity under free-living conditions: A systematic review. Nature Publishing Group; 2016.

[9] Paraschiakos S, de Sá CR, Okai J, Slagboom PE, Beekman M, Knobbe A. A recurrent neural network architecture to model physical activity energy expenditure in older people. Data Mining and Knowledge Discovery. 2022;36(1):477-512.

[10] Brage S, Westgate K, Franks PW, Stegle O, Wright A, Ekelund U, et al. Estimation of free-living energy expenditure by heart rate and movement sensing: A doubly-labelled water study. PLoS ONE. 2015;10(9).

[11] Altini M, Penders J, Vullers R, Amft O. Estimating Energy Expenditure Using Body-Worn Accelerometers: A Comparison of Methods, Sensors Number and Positioning. IEEE Journal of Biomedical and Health Informatics. 2015;19(1):219-26.

[12] HIBBING PR, LAMUNION SR, KAPLAN AS, CROUTER SE. Estimating Energy Expenditure with ActiGraph GT9X Inertial Measurement Unit. Medicine & Science in Sports & Exercise. 2018;50(5).

[13] O'Driscoll R, Turicchi J, Beaulieu K, Scott S, Matu J, Deighton K, et al. How well do activity monitors estimate energy expenditure? A systematic review and meta-analysis of the validity of current technologies. British Journal of Sports Medicine. 2020 3;54(6):332 LP 340.

[14] Pontzer H, Yamada Y, Sagayama H, Ainslie PN, Andersen LF, Anderson LJ, et al. Daily energy expenditure through the human life course. Science. 2021 8;373(6556).

[15] Westerterp KR. Control of energy expenditure in humans; 2017.

[16] CardioBAN kit;. Available from: https://www.pluxbiosignals.com/products/cardioban.

[17] Altini M, Penders J, Amft O. Energy Expenditure Estimation Using Wearable Sensors: A New Methodology for Activity-Specific Models. In: Proceedings of the Conference on Wireless Health. WH '12. New York, NY, USA: Association for Computing Machinery; 2012. .

[18] Brazier JE, Harper R, Jones NMB, O'Cathain A, Thomas KJ, Usherwood T, et al. Validating the SF-36 health survey questionnaire: New outcome measure for primary care. British Medical Journal. 1992;305(6846):160-4.

[19] Craig CL, Marshall AL, Sjöström M, Bauman AE, Booth ML, Ainsworth BE, et al. International physical activity questionnaire: 12-Country reliability and validity. Medicine and Science in Sports and Exercise. 2003 8;35(8):1381-95.

[20] Movella DOT;. Available from: https://www.movella.com/products/wearables/movella-dot.

[21] Empatica E4;. Available from: https://www.empatica.com/en-eu/research/e4/.

[22] Freestyle Libre 3;. Available from: https://www.freestyle.abbott/nl-nl/producten/freestylelibre-3.html.

[23] DeBlois JP, White LE, Barreira TV. Reliability and validity of the COSMED K5 portable metabolic system during walking. European Journal of Applied Physiology. 2021 1;121(1):209-17.

[24] Fullmer S, Benson-Davies S, Earthman CP, Frankenfield DC, Gradwell E, Lee PSP, et al. Evidence Analysis Library Review of Best Practices for Performing Indirect Calorimetry in Healthy and Non-Critically Ill Individuals. Journal of the Academy of Nutrition and Dietetics. 2015;115(9):1417-46.

[25] Nösslinger H, Mair E, Toplak H, Hörmann-Wallner M. Underestimation of resting metabolic rate using equations compared to indirect calorimetry in normal-weight subjects: Consideration of resting metabolic rate as a function of body composition. Clinical Nutrition Open Science. 2021;35:48-66.

[26] Álvarez-García JA, Cvetkovic B, Lustrek M. A survey on energy expenditure estimation using wearable devices. ACM Computing Surveys. 2020 9;53(5).

[27] Compher C, Frankenfield D, Keim N, Roth-Yousey L. Best Practice Methods to Apply to Measurement of Resting Metabolic Rate in Adults: A Systematic Review. Journal of the American Dietetic Association. 2006;106(6):881-903.

[28] Thoonen M, Veltink P, Halfwerk F, Van Delden R, Wang Y. A Movement-Artefact-Free Heart-Rate Prediction System. In: Computing in Cardiology. vol. 2022-Septe; 2022. Available from: https://www.utwente.nl/en/techmed/facilities/htwb-.

[29] Aranburu A. IMU Data Processing to Recognize Activities of Daily Living with Smart Headset Permalink. Available from: https://escholarship.org/uc/item/5rs5t0sf.

[30] Chiari L, Avanzolini G, Ursino M. A comprehensive simulator of the human respiratory system: Validation with experimental and simulated data. Annals of Biomedical Engineering. 1997;25(6):985-99.

[31] Fincham WF, Tehrani FT. A mathematical model of the human respiratory system. Journal of Biomedical Engineering. 1983 4;5(2):125-33.

[32] Rebuck AS, Slutsky AS, Mahutte CK. A mathematical expression to describe the ventilatory response to hypoxia and hypercapnia. Respiration Physiology. 1977;31(1):107-16.

[33] Wijayasiri L, McCombe K. Alveolar gas equation. In: The Primary FRCA Structured Oral Examination Study Guide 1. StatPearls Publishing; 2020. p. 31-2.

[34] Weir JBdV. New methods for calculating metabolic rate with special reference to protein metabolism. The Journal of Physiology. 1949 8;109(1-2):1-9.

[35] Ndahimana D, Kim EK. Measurement Methods for Physical Activity and Energy Expenditure: a Review. Clinical Nutrition Research. 2017;6(2):68.

[36] Scott C. Misconceptions about Aerobic and Anaerobic Energy Expenditure. Journal of the International Society of Sports Nutrition. 2005 12;2(2):32-7.

[37] Rutkowski DR, Barton GP, François CJ, Aggarwal N, Roldán-Alzate A. Sex differences in cardiac flow dynamics of healthy volunteers. Radiology: Cardiothoracic Imaging. 2020 2;2(1).

[38] Plagenhoef S, Gaynor Evans F, Abdelnour T. Anatomical Data for Analyzing Human Motion. Research Quarterly for Exercise and Sport. 1983;54(2):169-78.

[39] Jones E, Oliphant T, Peterson P. SciPy: Open Source Scientific Tools for Python; 2001. Available from: `http://www.scipy.org/`.

[40] Barclay CJ. Chapter 6 - Efficiency of Skeletal Muscle. Academic Press; 2019. p. 111-27.

[41] Barclay CJ, Curtin NA. Advances in understanding the energetics of muscle contraction; 2023.

[42] Heil DP. Predicting Activity Energy Expenditure Using the Actical® Activity Monitor. Research Quarterly for Exercise and Sport. 2006 3;77(1):64-80.

[43] Van Hees VT, Van Lummel RC, Westerterp KR. Estimating activity-related energy expenditure under sedentary conditions using a tri-axial seismic accelerometer. Obesity. 2009;17(6):1287-92.

[44] Amaro-Gahete FJ, Sanchez-Delgado G, Alcantara JMA, Martinez-Tellez B, Acosta FM, Merchan-Ramirez E, et al. Energy expenditure differences across lying, sitting, and standing positions in young healthy adults. PLoS ONE. 2019 6;14(6).

[45] Pires IM, Marques G, Garcia NM, Flórez-Revuelta F, Teixeira MC, Zdravevski E, et al. Pattern recognition techniques for the identification of activities of daily living using a mobile device accelerometer. Electronics (Switzerland). 2020;9(3).

[46] Nguyen H, Lebel K, Bogard S, Goubault E, Boissy P, Duval C. Using Inertial Sensors to Automatically Detect and Segment Activities of Daily Living in People with Parkinson's Disease. IEEE Transactions on Neural Systems and Rehabilitation Engineering. 2018 1;26(1):197-204.

[47] Hong LC, Tee C, Goh MKO. Activities of Daily Living Recognition Using Deep Learning Approaches. Journal of Logistics, Informatics and Service Science. 2022;9(4):129-48.

[48] Ortiz-Prado E, Dunn JF, Vasconez J, Castillo D, Viscor G. Partial pressure of oxygen in the human body: a general review. American journal of blood research. 2019;9(1):1-14.

[49] Urbanchek MG, Picken EB, Kalliainen LK, Kuzon WM. Specific Force Deficit in Skeletal Muscles of Old Rats Is Partially Explained by the Existence of Denervated Muscle Fibers. The Journals of Gerontology: Series A. 2001 5;56(5):B191-7.